HIV-1 Vpr-induced DNA damage activates NF-κB independent of cell cycle arrest and CRL4A^{DCAF1} engagement

Carina Sandoval[1] and Oliver I. Fregoso[1,2]

[1] Molecular Biology Institute, University of California, Los Angeles, California, USA
[2] Department of Microbiology, Immunology, and Molecular Genetics, University of California, Los Angeles, California, USA

Correspondence: Oliver I. Fregoso
Tel: 310.794.1424
Email: ofregoso@mednet.ucla.edu

ABSTRACT

Lentiviral accessory genes enhance replication through diverse mechanisms. HIV-1 accessory protein Vpr modulates the host DNA damage response (DDR) at multiple steps through the degradation of host proteins, cell cycle arrest, DNA damage, and both activation and repression of DDR signaling. Vpr also alters host and viral transcription; however, the connection between Vpr-mediated DDR modulation and transcriptional activation remains unclear. Here, we determined the cellular consequences of Vpr-induced DNA damage using Vpr mutants that allow us to separate the ability of Vpr to induce DNA damage from $CRL4A^{DCAF1}$ complex dependent phenotypes including cell cycle arrest, host protein degradation, and repression of DDR. In both tissue-cultured U2OS cells and primary human monocyte-derived macrophages (MDMs), we found that Vpr induces DNA breaks and activates DDR signaling in the absence of cell cycle arrest and $CRL4A^{DCAF1}$ complex engagement. Moreover, through RNA-sequencing, we found that Vpr-induced DNA damage alters cellular transcription via activation of NF-κB/RelA signaling. NF-κB/RelA transcriptional activation was dependent on ATM-NEMO, as inhibition of NEMO resulted in loss of NF-κB transcriptional upregulation by Vpr. Furthermore, HIV-1 infection of primary MDMs validated NF-κB transcriptional activation during infection. Both virion delivered and *de novo* expressed Vpr induced DNA damage and activated NF-κB transcription, suggesting that engagement of the DDR can occur during early and late stages of viral replication. Together, our data support a model where Vpr-induced DNA damage activates NF-κB through the ATM-NEMO pathway, independent of cell cycle arrest and $CRL4A^{DCAF1}$ engagement. We propose this is essential to overcoming restrictive environments, such as macrophages, to enhance viral transcription and replication.

38 **INTRODUCTION**

39

40 The DDR is a signaling cascade activated in response to exogenous and endogenous genotoxic
41 stress, such as DNA breaks. The DDR consists of sensor proteins that sense the damaged DNA,
42 mediator and transducer proteins that transmit the signal of damaged DNA, and effector proteins
43 that elicit a cellular response. Typically, the DDR is divided into three main pathways based on
44 the mediator kinases activated: Ataxia telangiectasia and Rad3 related (ATR), ataxia
45 telangiectasia mutated (ATM), and DNA-dependent protein kinase (DNA-PK). Single-strand DNA
46 breaks (SSBs) are primarily sensed by RPA to activate ATR signaling, while double-strand DNA
47 breaks (DSBs) can be sensed by the MRN (MRE11, RAD51, and NBS1) or Ku70/80 complexes
48 to activate either ATM or DNA-PK signaling, respectively (1,2). However, a significant amount of
49 crosstalk exists between these pathways. DDR signaling leads to various cellular responses, such
50 as DNA repair, cell cycle arrest (3), transcriptional changes (4,5), apoptosis, or senescence (6).

51

52 Many diverse RNA and DNA viruses have evolved to modulate the DDR to enhance viral
53 replication (7,8). Primate lentiviruses, such as HIV-1, primarily engage the DDR through the
54 accessory protein Vpr (9,10). Vpr is evolutionarily conserved amongst extant primate lentiviruses
55 and is required for replication *in vivo* (11,12) and in macrophage (13,14) and dendritic cells (15)
56 *in vitro*. Vpr is largely unique among the lentiviral accessory genes in that it is delivered by the
57 incoming virion, allowing it to act early in viral replication, and is also expressed *de novo* from the
58 integrated provirus, allowing it to act later in viral replication (16). Although the primary conserved
59 function of Vpr remains elusive, viruses lacking Vpr have decreased proviral transcription in
60 monocyte derived macrophages (MDMs) and dendritic cells (15), suggesting an important role for
61 Vpr in viral transcription.

62

63 Emerging literature suggests that Vpr engages the DDR at multiple, potentially unique, steps.
64 ATR activation by Vpr leads to cell cycle arrest and requires recruitment of the $CRL4A^{DCAF1}$
65 complex, which has a primary role in DNA repair (17). $CRL4A^{DCAF1}$ complex recruitment by Vpr
66 also leads to the degradation of many host proteins involved in the DDR, including CCDC137
67 (18), HLTF (19), UNG2 (20,21), SAMHD1 (22), Mus81/EME1 (23), EXO1 (24), TET2 (25), and
68 MCM10 (26), as well as more global proteome remodeling (27). Moreover, $CRL4A^{DCAF1}$ complex
69 recruitment is required for Vpr-mediated repression of DSB repair (28). In contrast, we have
70 previously shown that the ability of Vpr to induce DNA damage does not correlate with cell cycle

arrest or repression of DSB repair (28), suggesting that Vpr-induced DNA damage may have unique roles in enhancing lentiviral replication.

Both DNA damage and HIV-1 Vpr promote transcriptional changes involving NF-κB (29,30). In response to DSBs, ATM signaling promotes NF-κB transcriptional upregulation through the ATM-NEMO pathway (31). ATM and NEMO interact in the nucleus before translocating to the cytoplasm (32,33) to subsequently activate RelA nuclear translocation, promoter binding, and NF-κB transcriptional activation. Previous literature suggests that HIV-1 Vpr modulates NF-κB pathways through phosphorylation and ubiquitylation of TAK1 to enhance NF-κB signaling (34) and altering the availability of the NF-κB p50-RelA heterodimer to inhibit NF-κB signaling (35). This proposes a testable model where Vpr-induced DNA damage alters the cellular environment to enhance viral replication by altering transcription through ATM-NEMO and NF-κB. Here, we aimed to identify the cellular consequences of Vpr-induced DNA damage and the connection between DNA damage and ATM activation, CRL4A^{DCAF1} engagement, and transcriptional changes.

To determine the consequences of Vpr-induced DNA damage on cellular transcription, we used Vpr mutants that allow us to uncouple DNA damage from cell cycle arrest and CRL4A^{DCAF1} complex mediated host protein degradation. We found that Vpr does not require CRL4A^{DCAF1} engagement to induce DNA breaks and activate DDR signaling in U2OS tissue-culture cells and primary human MDMs. RNA-sequencing (RNA-seq) identified that wild-type HIV-1 Vpr and Vpr mutants that do not induce cell cycle arrest or engage the CRL4A^{DCAF1} complex alter NF-κB associated cellular transcription. In support of this, we showed that only Vpr proteins that induce DNA damage activate RelA nuclear translocation and upregulate NF-κB target genes, such as BIRC3 and CXCL8. We further assessed the requirement for ATM and NEMO signaling in Vpr-mediated NF-κB activation. We found that inhibition of NEMO resulted in loss of NF-κB transcriptional upregulation in primary MDMs. HIV-1 infection and virus-like particle (VLP) delivery of Vpr in MDMs validated the upregulation of NF-κB target genes early during infection. Together, our data support a model where Vpr-induced DNA damage activates NF-κB through the ATM-NEMO pathway, independent of cell cycle arrest and CRL4A^{DCAF1} complex mediated host protein degradation. This study further informs how lentiviral accessory proteins engage the DDR at multiple and unique steps, which remodels host environment and immune pathways to promote viral replication.

105 **RESULTS**

106

107 **HIV-1 Vpr induces DNA damage and alters cellular transcription independent of**
108 **CRL4A^{DCAF1} engagement and cell cycle arrest**

109 Given the connections between the DDR and cellular transcription, we set out to understand
110 whether the ability of Vpr to induce DNA damage gives rise to transcriptional changes, and
111 whether these transcriptional changes are distinct from those caused by Vpr-mediated cell cycle
112 arrest and/or degradation of host proteins. We have previously shown that a Vpr mutant that is
113 unable to cause cell cycle arrest (HIV-1 Q23-17 S79A) causes DNA damage (28). However this
114 mutant still engages the DCAF1 component of the CRL4A^{DCAF1} E3 ubiquitin ligase complex (36).
115 To test the connection between transcriptional changes, cell cycle arrest, and host protein
116 degradation, we used the HIV-1 Q23-17 Vpr mutant H71R, which does not bind the DCAF1
117 component of the CRL4A^{DCAF1} E3 ubiquitin ligase complex and thus loses the ability to cause cell
118 cycle arrest and degrade host proteins (28) (Fig. S1A). U2OS cells were infected with rAAV
119 expressing either HIV-1 Q23-17 Vpr wild type (WT), Vpr H71R, Vpr Q65R, a mutant of Vpr that is
120 largely functionally dead (37), or etoposide (positive control). DDR activation was assessed by
121 immunofluorescence while DNA damage was assessed by the comet assay 24 hours post
122 infection. Consistent with our previous results, HIV-1 Vpr WT induces DNA breaks (Fig. 1A) and
123 activates the DDR marker γH2A.x (Fig. 1B), while the nonfunctional Q65R mutant does not. In
124 addition, we found that H71R induces DNA breaks (Fig. 1A) and activates γH2A.x (Fig. 1B) at
125 levels similar to Vpr WT. To validate this, we knocked-down DCAF1 in U2OS cells with shRNAs
126 and found that Vpr can still induce DNA breaks and activate DDR signaling when DCAF1 is
127 knocked down (Fig. S1B-D). Together, our data show that Vpr does not require DCAF1 or
128 associated cellular responses to induce DNA damage and activate the DDR, and that the H71R
129 Vpr mutant allows us to investigate the ability of Vpr to induce DNA damage in the absence of
130 host protein degradation and cell cycle arrest.

131

132 Next, we asked if Vpr mutants that induce DNA damage in the absence of cell cycle arrest (H71R
133 and S79A) and CRL4A^{DCAF1} recruitment (H71R) alter cellular transcription. U2OS cells were
134 infected with rAAV expressing HIV-1 Vpr WT, H71R, S79A, and Q65R, and RNA was collected
135 at 12, 24, and 36 hours post infection. RNA-seq identified that Vpr WT, H71R and S79A, but not
136 Q65R or empty vector, significantly alter cellular transcription 36 hours post infection when
137 compared to untreated cells (Fig. 1C-E and Fig. S2A-B). Sixty-eight differentially expressed genes
138 with pvalue <0.01 and FDR < 4.50E-05 were shared among Vpr WT, H71R, and S79A, indicative

139 of genes potentially altered by Vpr-induced DNA damage (Fig. 1D and 1E). Gene ontology
140 indicated the shared upregulated genes were enriched for positive regulation of NF-κB signaling
141 and NF-κB signaling pathways, and transcriptional regulatory relationships unravelled by
142 sentence-based text-mining (TRRUST) analysis (38) further identified RelA/NF-κB as a top
143 transcription factor activated by Vpr (Fig. 1F-G, Fig. S2 A-B and Supplemental Files S1 & S2).
144 Finally, we identified differentially expressed genes exclusively altered in Vpr WT expressing cells,
145 Vpr WT and S79A expressing cells, and unique to both Vpr H71R and S79A mutant expressing
146 cells (Supplemental Files S1 & S2). Collectively, our data show that Vpr alters cellular
147 transcription in the absence of cell cycle arrest and host protein degradation, and further suggest
148 that Vpr-induced DNA damage specifically alters RelA/NF-κB-mediated transcription.
149
150 **HIV-1 Vpr-induced DNA damage activates RelA and promotes NF-κB transcription**
151 We next directly assayed whether Vpr mutants that can only induce DNA damage activate
152 RelA/NF-κB. NF-κB activation was first validated by qRT-PCR for two NF-κB target genes
153 identified in our RNA-seq, BIRC3 and CXCL8 (Fig. 1E), which are important for innate immunity
154 and cell survival (39,40). U2OS cells were infected with rAAV expressing Vpr WT, H71R and
155 Q65R for 24 or 36 hours. Consistent with the RNA-seq, Vpr WT and H71R upregulate BIRC3 and
156 CXCL8 compared to untreated cells or Q65R mutant (Fig. 2A). qRT-PCR for BIRC3 and CXCL8
157 in DCAF1 knock-down cells further confirmed that DCAF1 recruitment is not required for HIV-1
158 Vpr to activate these two NF-κB target genes (Fig. S1E). To directly assess NF-κB activation, we
159 assayed for RelA localization by immunofluorescence. As RelA is cytoplasmic when inactive and
160 nuclear when active, we expect that Vpr WT and H71R will lead to nuclear translocation of RelA.
161 Indeed, we found that Vpr WT and H71R activate nuclear translocation of RelA similar to the
162 positive control, etoposide, while Vpr Q65R and empty vector do not (Fig 2B). These data
163 demonstrate that Vpr activates RelA and NF-κB transcription in the absence of cell cycle arrest,
164 DCAF1 recruitment and host protein degradation, suggesting that Vpr-induced DNA damage is
165 sufficient to drive NF-κB activation.
166
167 **HIV-1 Vpr-induced DNA damage activates ATM-NEMO signaling**
168 NF-κB is activated in response to many pathways and signals involved in DNA repair and innate
169 immunity (41). One such pathway is ATM-NEMO, where ATM stimulates NEMO to activate RelA
170 and thus NF-κB signaling (33). Previous work has shown that Vpr activates markers of both ATR
171 and ATM signaling (28,42). While ATR is required for Vpr-induced cell cycle arrest, the extent of
172 ATM activation and the cellular consequences of ATM activation without cell cycle arrest are

173 unclear. We hypothesized that Vpr-induced DNA damage activates the ATM-NEMO pathway,
174 which consequently promotes RelA/NF-κB transcription. To determine if Vpr-induced DNA
175 damage activates ATM signaling in the absence of cell cycle arrest and DCAF1 recruitment, we
176 measured activation of multiple DDR proteins including two DNA damage sensors, NBS1 and
177 MRE11, and two downstream signaling transducers, 53BP1 and γH2A.x. U2OS cells stably
178 expressing NBS1-GFP or 53BP1-GFP were infected with rAAV expressing Vpr WT, H71R, and
179 Q65R to assess DDR activation through live-cell imaging throughout infection. We found that Vpr
180 WT and H71R promote the formation of NBS1 and 53PB1 foci at 26, 33, and 48 hours post
181 infection (hpi), similar to the positive control etoposide, while the non-functional Q65R Vpr mutant
182 was indistinguishable from untreated control cells (Fig. 3A and Fig. S3A-C). As many viruses
183 activate or dysregulate DDR signaling through relocalization or sequestration of markers of the
184 DDR, we next assayed for colocalization of the DNA damage sensors MRE11 and NBS1, and
185 transducers 53BP1 and γH2A.x. Both damage sensors MRE11 and NBS1, and transducers
186 53PB1 and γH2A.x, colocalize in Vpr WT and H71R, similar to etoposide treated cells (Fig. 3B&C),
187 suggesting that Vpr-induced DNA damage activates, but does not dysregulate, classical ATM
188 signaling.
189
190 To determine if NEMO is required for Vpr to upregulate NF-κB transcription, we inhibited NEMO
191 using a cell-permeable NEMO binding domain (NBD) inhibitor peptide (43). U2OS cells were
192 pretreated with NBD peptide and infected with rAAV expressing Vpr WT and mutants. We
193 assessed upregulation of the NF-κB target genes BIRC3 and CXCL8 using qRT-PCR. As before,
194 Vpr WT and H71R upregulated both BIRC3 and CXCL8, while Q65R and empty vector did not
195 (Fig. 4). With the addition of the NBD, Vpr WT and H71R mutant lost the ability to upregulate
196 BIRC3 and CXCL8 (Fig. 4), suggesting that Vpr requires NEMO activation to upregulate
197 transcription of NF-κB target genes.
198
199 **Virion delivery of Vpr, through VLPs or HIV-1 ΔENV infection, in primary MDMs activates**
200 **ATM-NEMO signaling and promotes RelA/NF-κB transcription**
201 Together our data proposes a model where Vpr-induced DNA damage activates ATM and NEMO
202 signaling resulting in RelA nuclear translocation and NF-κB transcriptional upregulation. We next
203 tested this model in primary human MDMs, where Vpr enhances viral transcription and replication
204 (14). Primary MDMs (Fig. S4A) were infected with virus-like particles (VLPs) carrying
205 physiological levels of Vpr WT, H71R, or Q65R (Fig. S4B), and assayed for DNA damage, NF-κB
206 activation, and NEMO dependence (Fig. 5A). Similar to overexpression of Vpr in U2OS tissue

207 culture cell lines, Vpr WT and H71R mutant induced DNA breaks and activated γH2A.x compared
208 to Vpr Q65R and empty VLPs (Fig. 5B-C). Consistent with our data in U2OS cells, Vpr WT and
209 H71R, but not Q65R or empty VLPs, upregulated BIRC3 and CXCL8 similar to the TNFα positive
210 control when compared to empty cells (Fig. 5D and Fig. S4C). Finally, NBD delivery prior to VLP
211 infection blocked Vpr WT and H71R-mediated BIRC3 and CXCL8 transcriptional activation, but
212 not Vpr-induced DNA damage (Fig. 5C-D and Fig. S4C). These data indicate that physiological
213 levels of virion-delivered Vpr induces DNA damage that activates NF-κB transcription in a NEMO
214 dependent manner in primary MDMs.
215
216 To determine if HIV-1 infection activates NF-κB target genes, we infected primary human MDMs
217 from six different donors with HIV-1 ΔEnv and assayed for transcriptional changes at early (8
218 hours), intermediate (16 hours), and late (24 and 48 hours) timepoints post infection. HIV-1
219 infection was monitored by flow cytometry for HIV-1 core proteins and qRT-PCR for unspliced
220 transcripts (Fig. S4D-E), while NF-κB activation was measured by qRT-PCR for CXCL8 and
221 BIRC3. TNFα was used as positive control (Fig. S4F). HIV-1 ΔEnv infection resulted in
222 upregulation of CXCL8 and BIRC3 in MDMs as early as 8hpi in all donors, despite some donor-
223 to-donor variability in the magnitude of upregulation (Fig. 5E and Fig. S4G-H), suggesting that
224 HIV-1 infection upregulates Vpr-induced NF-κB target genes early during infection, consistent
225 with VLP delivery of Vpr. Jointly, our data support a model where both incoming HIV-1 Vpr and
226 *de novo* produced Vpr induces DNA damage that activates ATM-NEMO signaling to upregulate
227 NF-κB transcription (Fig. 6).
228
229 **DISCUSSION**
230
231 In this study, we tested the hypothesis that HIV-1 Vpr alters cellular transcription through induction
232 of DNA damage and activation of DDR signaling. By leveraging well-characterized Vpr mutants
233 that separate Vpr-induced DNA damage from cell cycle arrest and $CRL4A^{DCAF1}$ complex mediated
234 host protein degradation, we identified a current model where Vpr-induced DNA damage activates
235 ATM-NEMO signaling, which stimulates RelA and upregulates NF-κB mediated transcription.
236 Using U2OS and primary human MDMs, which allowed us for the first time to investigate how
237 HIV-1 Vpr engages the DDR in this important cell type, we showed that Vpr induces DNA breaks
238 and activates markers of ATM signaling independent of cell cycle arrest, $CRL4A^{DCAF1}$ complex
239 recruitment, and host protein degradation. Moreover, we showed that Vpr-induced DNA damage
240 correlates with RelA/NF-κB activation, as assayed by bulk RNA-seq, and RelA

241 immunofluorescence. We validated the upregulation of two NF-κB target genes, BIRC3 and
242 CXCL8, and showed that inhibition of NEMO ablates the ability of Vpr to upregulate NF-κB
243 transcription. Finally, VLP delivery of Vpr and HIV-1 infection show that incoming virion-
244 associated Vpr is sufficient to induce DNA damage and activate RelA/NF-κB transcription. In
245 complement, rAAV expression of Vpr show that *de novo* expressed Vpr can also induce DNA
246 damage and activate RelA/NF-κB transcription. These data suggest that Vpr-induced DNA
247 damage can play roles in both early and late stages of viral replication. Overall, our data support
248 a model where Vpr-induced DNA damage activates ATM-NEMO signaling and upregulates
249 RelA/NF-κB transcription in cell lines and primary human MDMs.
250
251 Although Vpr is a multifunctional and enigmatic protein, the DNA damage response is central to
252 many of the phenotypes associated with Vpr. Previous reports from our lab and others have
253 worked to untangle how and why Vpr engages the DDR. A consensus is emerging that Vpr
254 engages the DDR at multiple, potentially unique, steps. Through recruitment of the $CRL4A^{DCAF1}$
255 ubiquitin ligase complex, Vpr degrades various DDR proteins, activates ATR signaling, represses
256 double-strand DNA break repair, and causes cell cycle arrest (28,44). However, as shown here,
257 Vpr induces DNA damage and alters cellular transcription independent of its ability to engage the
258 $CRL4A^{DCAF1}$ ubiquitin ligase complex and associated phenotypes. Functions independent of host
259 protein degradation are unique among most lentiviral accessory genes, as their typical primary
260 functions depend on subverting antiviral mechanisms through host protein degradation (45).
261 These data further define the multifunctional nature of Vpr in enhancing lentiviral infection and
262 support the model where Vpr engages the DDR at multiple independent steps.
263
264 Here, we have also shown that Vpr-induced DNA damage directly correlates with NF-κB
265 transcriptional activation that is dependent on ATM signaling. We have demonstrated that Vpr
266 activates markers of ATM signaling, such as MRE11, NBS1, γH2A.x, and 53PB1, in a manner
267 that resembles host activation rather than dysregulation. Antagonism or dysregulation of DNA
268 damage sensors through relocalization or sequestration is a conserved mechanism among many
269 viruses to evade innate immune detection (46). While we have shown that Vpr-induced DNA
270 damage activates markers of ATM signaling in a manner that seems to facilitate classical ATM
271 activation, with the end goal of activating transcription, it remains to be seen whether Vpr-
272 mediated activation of ATR, which correlates with $CRL4A^{DCAF1}$ recruitment and cell cycle arrest,
273 is classically activated or dysreglated. Moreover, how Vpr induces DNA breaks leading to both
274 ATM and ATR activation is not understood.

275

276 Complementary studies have shown that Vpr modulates cellular (47) and viral transcription
277 (48,49). In the context of cellular transcription, Vpr activates genes associated with innate
278 immunity and proliferation in CD4+ T cells (50) and promotes the expression of proinflammatory
279 cytokines in MDMs and monocyte-derived dendritic cells (MDDCs) (15,25). Together this
280 suggests that Vpr has a vital role in transcriptional reprogramming to potentially create a
281 proinflammatory environment that is conducive for viral replication. Consistent with these studies,
282 we identified by bulk RNA-seq that Vpr regulates innate immune pathways that are either
283 independent of or dependent on cell cycle arrest and CRL4A^{DCAF1} engagement and host protein
284 degradation. Our data show that Vpr downregulates TASOR target genes (Fig. S2 D-F), which is
285 consistent with the literature suggesting that SIV and HIV-2 Vpr counteract the human silencing
286 hub (HUSH) repressor complex (51,52). Furthermore, we found that Vpr downregulates CXCL14,
287 which aligns with the data reporting that human papillomaviruses downregulate CXCL14 to
288 enhance replication (53).

289

290 Our data also indicate that Vpr activates the RelA/NF-κB immune pathway without induction of
291 cell cycle arrest and CRL4A^{DCAF1} recruitment and host protein degradation. This is consistent with
292 previous reports showing that Vpr activates NF-κB transcription via phosphorylation of TAK1 (34),
293 an upstream regulator of NF-κB. We further found that Vpr-induced DNA damage activates ATM-
294 NEMO signaling to upregulate RelA/NF-κB transcription, adding to the mechanistic understanding
295 of NF-κB activation by Vpr. Through engagement with the CRL4A^{DCAF1} complex, Vpr has also
296 been found to repress NF-κB activation by altering the availability of the NF-κB p50-p65
297 heterodimer, thus limiting proinflammatory cytokine expression (35). While it remains unclear
298 what differentiates Vpr-mediated NF-κB activation from repression, whether Vpr engages the
299 CRL4A^{DCAF1} complex seems to be a distinguishing factor. Furthermore, it is clear that in all cases
300 Vpr carefully modulates NF-κB activation without globally activating interferon, which would inhibit
301 viral replication. Thus, further studies understanding how Vpr manages to activate only aspects
302 of NF-κB signaling (54,55) will help to define how Vpr may contribute to the ability of HIV to subvert
303 the innate immune response.

304

305 Although various studies have shown that Vpr also alters viral transcription the mechanisms are
306 unclear and disparate. For example, Vpr-mediated LTR activation is associated with cell cycle
307 arrest where the LTR is most transcriptionally active (56,57), degradation of host proteins such
308 as CCDC137 (18), and CRL4A^{DCAF1} independent mechanisms (58). However, studies have

309 shown that Vpr also promotes LTR transcription in noncycling cells (59,60) where induction of cell
310 cycle arrest is absent and the necessity for degradation of specific host proteins in LTR activation
311 has not been extensively examined. One benefit of Vpr activating NF-κB signaling via ATM is the
312 potential direct enhancement of LTR transcription, as the HIV-1 LTR contains multiple NF-κB
313 binding sites essential for viral gene expression. In addition to NF-κB, we further identified that
314 Vpr activates CEBPB and JUN transcription factors involved in LTR activation. This is similar to
315 Vpr-mediated de-repression of the LTR by removal of the transcriptional repressor ZBTB2
316 following ATR activation (61). Overall, Vpr WT and mutants that induce only DNA damage globally
317 alter cellular transcription, upregulate NF-κB signaling and transcription factors that promote LTR-
318 driven transcription, suggesting that Vpr-induced DNA damage is important for promoting LTR
319 transcription to enhance viral replication.
320
321 Overall, our data suggest that during HIV infection, incoming Vpr and *de novo* expressed Vpr
322 prime the cellular environment by activating RelA/NF-κB signaling to promote LTR transcription
323 and enhance viral replication in macrophages. Our data align with the growing body of literature
324 that supports the role of accessory proteins modulating the host environment and the DDR to
325 promote viral replication through mechanisms independent of host protein degradation.

326 **FIGURE LEGENDS**

327

328 **Figure 1: HIV-1 Vpr induces DNA damage and alters cellular transcription independent of**
329 **cell cycle arrest and CRL4A^{DCAF1} engagement.** (A) Comet assay of U2OS cells infected with
330 rAAV expressing 3xFLAG-tagged Vpr WT, H71R, Q65R, untreated (negative control), or 50uM
331 etoposide (positive control). Percent tail DNA was quantified at 24 hours post infection (hpi) using
332 the OpenComet plug-in for the ImageJ software. Each circle represents one cell. N=3, one
333 representative experiment shown. (B) Representative immunofluorescence images of U2OS cells
334 infected under the same conditions as Fig. 1A; γH2A.x (magenta) and nuclei stained with DAPI
335 (blue). Images were taken at 63x magnification. N=3, one representative experiment shown. EV,
336 empty vector. (C) RNA-seq of U2OS cells at 36 hpi. Heat map displays Log_2 fold changes of
337 upregulated genes in red and downregulated genes in blue. Each column represents a biological
338 replicate, n=3 (D) Venn diagram of the top 100 upregulated and top 100 downregulated genes
339 among Vpr WT, S79A, H71R, and Q65R. E) Dot plot of the 68 conserved differentially expressed
340 genes among Vpr WT, S79A, and H71R. BIRC3 and CXCL8 are highlighted as the two most
341 upregulated genes (Log_2 fold change) under all conditions. (F) Gene ontology and (G) TRRUST
342 analysis of the 30 upregulated genes performed with Metascape software. Asterisk indicate
343 statistical significance compared to untreated control, as determined by one-way ANOVA test
344 (NS, nonsignificant; *** P< 0.0004, **** P< 0.0001). Related to Figures S1 and S2.

345

346 **Figure 2: HIV-1 Vpr activates RelA and promotes NF-κB transcription independent of cell**
347 **cycle arrest and CRL4A^{DCAF1} engagement.** (A) qRT-PCR validation of upregulated NF-κB target
348 genes BIRC3 and CXCL8. Normalized expression (ΔΔCt) was calculated by normalizing to
349 GAPDH followed by calculating fold change to untreated or empty vector treated cells. Cells
350 treated under the same conditions as Fig. 1C. n=3, one representative experiment shown. (B)
351 Representative immunofluorescence images of U2OS cells infected under the same conditions
352 as Fig. 1A; RelA (red) and nuclei stained with DAPI (blue). Images were taken at 63x
353 magnification. n=3, one representative experiment shown. Asterisk indicate statistical significance
354 compared to untreated control, as determined by one-way ANOVA test (NS, nonsignificant; ***
355 P< 0.0003, **** P< 0.0001).

356

357 **Figure 3: Vpr-induced DNA damage activates ATM signaling independent of cell cycle**
358 **arrest and CRL4A^{DCAF1} engagement.** (A) Live-cell imaging of U2OS cells stably expressing
359 NBS1-GFP or 53PB1-GFP. Cells were infected under the same conditions as Fig. 1A and

360 representative images were taken at 33 hpi at 63x magnification. n=3, one representative
361 experiment shown. (B) Representative images of co-localization of DNA damage sensors MRE11
362 (magenta) and NBS1 (yellow) in U2OS NBS1-GFP or (C) DNA damage transducers yH2A.x
363 (magenta) and 53PB1 (yellow) in U2OS 53PB1-GFP cells infected under the same conditions as
364 Fig. 1A. Representative images taken at 24 hpi at 63x magnification. n=3, one representative
365 experiment shown. Related to Figure S3.
366
367 **Figure 4: Vpr upregulates NF-κB transcription dependent on NEMO, yet independent of cell**
368 **cycle arrest and CRL4A^{DCAF1} engagement.** qRT-PCR of BIRC3 and CXCL8 in the presence or
369 absence of Nemo-Binding Inhibitor peptide (NBD) at 36 hpi. U2OS cells were pretreated with
370 100uM of NBD for 2 hours prior to infection with rAAV expressing 3xFLAG-tagged Vpr WT, H71R,
371 Q65R, empty vector (negative control). Normalized expression to GAPDH. Asterisk indicate
372 statistical significance compared to untreated control, as determined by one-way ANOVA test
373 (NS, nonsignificant; **** P< 0.0001).
374
375 **Figure 5: Vpr-induced DNA damage activates ATM-NEMO signaling and NF-κB**
376 **transcription in primary MDMs early during infection.** (A) Experimental schematic depicting
377 the isolation and differentiation of primary human monocyte-derived macrophages (MDMs) from
378 peripheral blood mononuclear cells (PBMCs) followed by delivery of Vpr via Virus-like Particles
379 (VLPs) or HIV-1 infection. Infected MDMs were assayed for induction of DNA damage, activation
380 of DDR signaling, and the upregulation of NF-κB target genes in the context of NEMO inhibitor.
381 (B) Comet assay of MDMs treated with VLPs packaging 3xFLAG-tagged Vpr WT, H71R, Q65R,
382 empty VLPs (negative control), or 25uM Mitomycin C (positive control) for 8 hours. Comet assay
383 analysis was performed as in Fig. 1A. n=2, one representative experiment shown. (C)
384 Representative immunofluorescence images of MDMs infected with VLPs as in Fig. 5B and
385 treated or not with Nemo-Binding Inhibitor peptide (NBD); γH2A.x (magenta) and nuclei stained
386 with DAPI (blue). Images were taken at 100x magnification. n=3, one representative experiment
387 shown. (D) qRT-PCR for CXCL8 of MDMs treated with NBD as in Fig. 5C with TNFα as positive
388 control. n=3, one representative experiment shown. (E) qRT-PCR for CXCL8 of MDMs infected
389 with HIV-1 ΔEnv for 8, 16, 24, and 48 hpi from four separate donors. Normalized expression to
390 GAPDH. Asterisk indicate statistical significance compared to untreated control, as determined
391 by one-way ANOVA test (NS, nonsignificant; * P<0.03, ** P < 0.005, **** P< 0.0001). Related to
392 Figure S4.
393

394 **Figure 6: Model showing Vpr-induced DNA damage activates ATM and NEMO signaling**
395 **resulting in RelA nuclear translocation and NF-κB transcriptional upregulation.** 1. Vpr
396 induces double-strand DNA breaks independent of cell cycle arrest and CRL4A^{DCAF1} complex
397 engagement. 2. Vpr-induced DNA damage activates markers of ATM signaling including MRE11,
398 NBS1, γH2A.x, and 53PB1. 3. ATM-DDR activation results in NEMO relieving RelA inhibition from
399 inhibitor of NF-κB (IκBα and IκBβ). 4. RelA translocates into the nucleus. 5. RelA binds to NF-κB
400 promoters and activates transcription (txn) of NF-κB target genes such as BIRC3 and CXCL8.
401 (Schematic made on Biorender).
402
403 **SUPPLEMENTAL FIGURE LEGENDS**
404
405 **Figure S1: Knockdown of DCAF1 does not abrogate the ability of Vpr to induce DNA**
406 **damage, activate DDR signaling, or upregulate NF-κB target genes.** (A) Schematic
407 representation of Vpr mutants used in these studies to decouple some Vpr functions. Vpr S79A
408 and Vpr H71R do not induce cell cycle arrest, and H71R also does not bind DCAF1 of the
409 CRL4A^{DCAF1} complex to degrade host proteins or remodel the proteome. Vpr Q65R (not shown)
410 is a largely non-functional negative control. (B) Western blot of endogenous DCAF1 U2OS cells
411 to test stable knockdown with shRNA. Control (ctl) shRNA and two DCAF1-specific shRNAs
412 (shRNA1 and shRNA2) were used. Actin is used as a loading control. (C) Comet assay of DCAF1
413 knock-down cells infected with rAAV and analyzed as in Fig. 1A. n=1. (D) Representative
414 immunofluorescence images of DCAF1 knock-down U2OS cells infected under the same
415 conditions as Fig. 1A.; γH2A.x (magenta) and nuclei with DAPI (blue). Images were taken at 63x
416 magnification. n=1, one representative image shown. (E) qRT-PCR for CXCL8 and BIRC3 in
417 DCAF1 knock-down U2OS cells infected under the same conditions as Fig. 1A. n=1. Asterisk
418 indicate statistical significance compared to untreated control, as determined by t-test (NS,
419 nonsignificant; * P< 0.02, ** P<0.004, *** P<0.0003, **** P<0.0001). EV, empty vector negative
420 control; Etop., etoposide positive control. Related to Figures 1 and 2.
421
422 **Figure S2: Vpr alters cellular transcription through diverse mechanisms that are either**
423 **dependent or independent of cell cycle arrest and CRL4A^{DCAF1} engagement.** (A) Gene
424 ontology using Metascape displaying TRRUST analysis for upregulated genes. (B) Principal
425 component analysis (PCA) of the RNA-seq data showing the relatedness of the three biological
426 replicates compared to empty vector or untreated cells. Related to Figure 1.
427

428 **Figure S3: Vpr-induced DNA damage activates markers of ATM signaling.** (A) Live-cell
429 imaging taken on the IncuCyte of U2OS NBS1-GFP or 53PB1-GFP cells infected as in Fig. 1A
430 for 48 hrs. n=2, one representative experiment shown. (B & C) Quantification of DNA damage
431 induced in the live-cell imaging experiment in Fig. 3A at 8, 26, 33, and 48hpi. Foci per cell and
432 foci size were quantified using ImageJ software. Images were taken at 63x magnification using
433 the LSM 900. n=3, one representative experiment shown. EV, empty vector; AU, arbitrary units.
434 Related to Figure 3.
435
436 **Figure S4: Infection of primary MDMs with VLPs packaging Vpr protein or HIV-1 infection**
437 **upregulate NF-κB transcription dependent on NEMO.** (A) Flow cytometry plots displaying
438 differentiation of PBMC-derived monocytes to macrophages. Primary MDMs are CD14+, CD45+
439 and CD16+. n=6, one representative experiment shown. (B) Western blot of 3X FLAG-Vpr WT
440 and mutants packaged in Virus-like particles (VLPs). (C) qRT-PCR for BIRC3 of MDMs treated
441 with NBD as in Fig. 5C with TNFα as positive control. n=3, one representative experiment shown.
442 (D) Histogram quantifying percent of infected MDMs with HIV-1 ΔEnv at 48hpi. n=6, one
443 representative experiment shown. (E) qRT-PCR for unspliced HIV-1 RNA at 8, 16, 24 and 48hpi.
444 n=6, one representative experiment shown. (F) qRT-PCR for TNFα of MDMs infected with HIV-1
445 ΔEnv at 8, 16, 24 and 48hpi. n=6, one representative experiment shown. (G & H) qRT-PCR for
446 BIRC3 or CXCL8 of MDMs infected with HIV-1 ΔEnv at 8, 16, 24 and 48hpi in separate donors.
447 n=6, (G) is all 6 donors, (H) is donors 5 and 6 in addition to those shown in Fig. 5E. Asterisk
448 indicate statistical significance compared to untreated control, as determined by one-way ANOVA
449 test (NS, nonsignificant; **** P<0.0001). Related to Figure 5.
450
451 **Files S1 & S2: HIV-1 Vpr WT and mutants alter cellular transcription.** Analysis of all
452 upregulated (File S1) and downregulated (File S2) genes in the RNA seq analysis that passes
453 statistical significance of Log2 (1.25), $p < 0.01$, and FDR < 4.50E-05. Counts per million reads
454 mapped (CPM) Log2 fold changes were calculated relative to untreated control. Related to Figure
455 1 and Figure S2.
456

457 **MATERIALS AND METHODS**

458

459 **Plasmids**

460 pcDNA-3xFLAG-Vpr and pscAAV-mCherry-T2A-Vpr WT and mutant plasmids were generated as
461 previously described (28). For rAAV production, pHelper and pAAV-2.5 capsid plasmids were
462 used (Addgene and (28). For VLP production, psPAX2 and pmD2.G were used (Addgene). For
463 HIV-1 ΔENV production, Bru-GFP ΔENV was generated as previously described (62) and
464 pmD2.G (Addgene). For lentivirus stable knock-down of DCAF1, pLKO.1 (Addgene),
465 psPAX2(Addgene) and pmD2.G (Addgene) were used.

466

467 **Generation of Viruses**

468 rAAV vectors packaging the pscAAV-mCherry-T2A-Vpr WT or mutant plasmids were generated
469 by transient transfection of HEK 293 cells using polyethyleneimine (PEI) as previously described
470 (63). Virus-like particles (VLPs) packaging Vpr WT or mutant proteins were generated by transient
471 transfection of HEK 293T using TransIT-LT1 (Mirus). VLPs were harvested 48hrs post
472 transfection, concentrated through a 25% sucrose cushion at 24,000 rpm for 3 hrs at 4˚C, and
473 resuspended in PBS. Protein packaging was validated through western blot. HIV-1 ΔENV
474 pseudotyped with VSV-G were generated by transient transfection of HEK 293T using TransIT-
475 LT1 (Mirus). Virus was collected 48hrs post transfection. Lentivirus expressing DCAF1 shRNAs
476 were generated by transfection of HEK 293T using TransIT-LT1 (Mirus).
477 shRNA1:
478 AATTCAAAAAGCTGAGAATACTCTTCAAGAACTCGAGTTCTTGAAGAGTATTCTCAGC
479 shRNA2:
480 AATTCAAAAAAGCACTTCAGATTATCATCAACTCGAGTTGATGATAATCTGAAGTGCT.
481 Media was changed 18 hours post transfection. Lentiviruses were harvested 48 hours post media
482 change and filtered through a 0.45 µm PES filter.

483

484 **Cell Lines and Cell Culture**

485 Human bone osteosarcoma epithelial (U2OS), Human embryonic kidney (HEK) 293, and HEK
486 293T cells were cultured as adherent cells directly on tissue culture plastic (Greiner) in Dulbecco's
487 modified Eagle's medium (DMEM) growth medium (high glucose, L-glutamine, no sodium
488 pyruvate; Gibco) with 10% fetal bovine serum (FBS) (Gibco) and 1% penicillin-streptomycin
489 (Gibco) at 37°C and 5% CO_2. All cells were harvested using 0.05% trypsin-EDTA (Gibco). The
490 panel of U2OS cells stably expressing 53PB1-GFP (64) and NBS1-GFP (65) were kindly provided

491 by Claudia Lukas (University of Copenhagen, Denmark). Stable DCAF1 knock-down cells were
492 generated by delivering lentiviruses expressing DCAF1 shRNAs or empty vector to U2OS cells.
493 U2OS with integrated lentiviral construct were selected for with 1ug/ml of Puromycin. Knock-down
494 of DCAF1 was assessed through western blots.
495
496 **Monocyte-Derived Macrophages (MDMs)**
497 Human peripheral blood mononuclear cells (PBMCs) were obtained from human donors at the
498 UCLA/CFAR Virology Core Laboratory. Primary monocytes were isolated from PBMCs by
499 negative selection using the EasySep™ Human T Cell Isolation Kit (STEM CELL) and were
500 differentiated into monocyte-derived macrophages (MDMs) by stimulation with 20ng/mL
501 macrophage colony-stimulating factor (M-CSF) (R&D Systems). MDMs were cultured in Roswell
502 Park Memorial Institute (RPMI) 1640 growth medium (L-Glutamine) with 10% fetal bovine serum
503 (Gibco) at 37°C and 5% CO_2 for 7 days while replenishing media every 3 days.
504
505 **Alkaline Comet Assay**
506 The alkaline comet assay and data analysis was performed as previously described (28), with
507 minor changes. MDMs were infected with VLPs delivering Vpr WT and mutants at equal protein
508 levels or 25uM Mitomycin C (Cayman). Cells were harvested with Accutase (STEM CELL) at 10
509 hrs post infection and resuspended in 0.5% low-melting-point agarose at 37°C. Images were
510 acquired on the Zeiss Axio Imager Z1. Images were analyzed using the OpenComet plug-in for
511 ImageJ.
512
513 **RNA-sequencing**
514 Total RNA from U2OS cells was isolated using TRIzol® reagent (Invitrogen). RNA integrity was
515 assessed using the Bioanalyzer TapeStation 4200 RNA High Sensitivity (Agilent). Library
516 Preparation was completed using the KAPA mRNA HyperPrep Kit (Illumina) enriching for Poly(A)
517 RNA with magnetic oligo-dT beads and attaching unique dual indexed adapters. Quality control
518 of the library was done with the Bioanalyzer TapeStation 4200 D1000 High Sensitivity (Agilent).
519 RNA was sequenced using the Hiseq3000 1x50 at the UCLA Technology Center for Genomics &
520 Bioinformatics core. Reads were aligned to the Human h38 STAR genome and gene counts were
521 determined using edgeR. log_2 reads per kilobase of transcript per million reads mapped (rpkms)
522 were calculated for samples compared to untreated cells. Heat map was generated using
523 pheatmap hierarchical clustering on z-score log2 rpkms. Gene ontology and TRRUST analysis
524 were done on Metascape.

525

526 **Quantitative Reverse Transcription PCR (qRT-PCR)**

527 Total RNA was isolated using the PureLink™ RNA Mini Kit (Invitrogen). RNA was reverse
528 transcribed using SuperScript IV First-Stand Synthesis System (Invitrogen) with Oligo(dT)
529 primers. qRT-PCR was performed with PowerTrack SYBR Green Master Mix (Thermo Fisher
530 Scientific) on the LightCycler 480 System (Roche) with the following primers (5' to 3') BIRC3
531 AAGCTACCTCTCAGCCTACTTT and CCACTGTTTTCTGTACCCGGA, CXCL8
532 TTTTGCCAAGGAGTGCTAAAGA and AACCCTCTGCACCCAGTTTTC, TNFα
533 CTCTTCTGCCTGCTGCACTTTG and ATGGGCTACAGGCTTGTCACTC, HIV-1 unspliced RNA
534 GCGACGAAGACCTCCTCAG and GAGGTGGGTTGCTTTGATAGAGA, and GAPDH
535 CAAGATCATCAGCAATGCCT and AGGGATGATGTTCTGGAGAG. mRNA levels were
536 quantified by calculating ΔΔCt. Target transcript Ct values were normalized to the Ct value of the
537 housekeeping gene GAPDH followed by calculating fold change to untreated or empty vector
538 treated cells.

539

540 **Live-Cell Imaging**

541 U2OS-53PB1-GFP and U2OS-NBS1-GFP cells were imaged using the IncuCyte S3 Live-Cell
542 Analysis Instrument (Sartorius). Mean Fluorescence Intensity (MFI) was calculated using the
543 Sartorius software. For higher resolution, U2OS-53PB1-GFP and U2OS-NBS1-GFP cells were
544 imaged using the LSM 900. Foci per cell and foci size were analyzed using ImageJ.

545

546 **Immunofluorescence**

547 Cells were plated in 6- or 24-well tissue culture plates (Greiner) and allowed to adhere overnight,
548 then infected with VLP (equal protein expression), rAAV-2.5 (1.4×10^8 copies/well), or etoposide
549 (Sigma). U2OS cells were permeabilized with 0.5% Triton X-100 in PBS at 4°C for 5 min and fixed
550 in 4% PFA for 20 min, MDM cells were permeabilized with 0.1% Saponin (Fisher) in PBS at 4°C
551 for 15 min and fixed in 4% PFA for 15 min. Cells were washed, incubated with blocking buffer (3%
552 BSA, 0.05% Tween 20, and 0.04 NaN_3 in PBS for U2OS cells or 3% FBS in 0.1% Saponin for
553 MDM cells) for 30 min. Cells were probed with appropriate primary antibodies (anti-γH2A.x
554 Ser139, anti-53BP1, or anti-RelA(p65) [Cell Signaling], anti-GFP [Takara], and anti-MRE11
555 [Novous]) and then washed and probed with Alexa Fluor-conjugated secondary antibodies (Life
556 Technologies). Nuclei were stained with diamidino-2-phenylindole (DAPI; Life Technologies).
557 Images were acquired on the LSM 980.

558

559 **Western Blots**

560 Protein was collected from cells as previously described (28). Membranes were blocked in
561 intercept blocking buffer (Li-COR Biosciences). Immunoblotting was performed using mouse anti-
562 FLAG M2 (Sigma-Aldrich), rabbit anti-Actin (Bethyl), or mouse anti-DCAF1 (Proteintech) for 1hr.
563 Blots were incubated with secondary antibodies IRDye 800CW anti-Rabbit and IRDye 680RD
564 anti-Mouse (Li-COR Biosciences) for 1 hr and then visualized using the Li-COR Odyssey M (Li-
565 COR Biosciences).

566

567 **HIV-1 ∆Env Infection**

568 MDMs were plated in 96-well tissue culture plates (Greiner) and allowed to adhere overnight.
569 MDMs underwent spinfection with HIV-1 ∆Env pseudotyped with VSV-G at 1200× *g* for 90 min at
570 37°C. Infection was assessed 48 hours after infection via qRT-PCR and Flow Cytometry.

571

572 **Flow Cytometry**

573 Isolated monocytes and infected MDMs were lifted from tissue culture plates using accutase
574 (STEM CELL). Cells were stained for CD14-FITC, CD45-APC, or CD16-APC (STEM CELL) for
575 30 min at 4°C, washed with PBS, fixed in 4% PFA for 15 min, permeabilized with 0.1% Triton X-
576 100 in PBS at 4°C for 15 min, then washed with PBS. Cells were probed for HIV-1 core antigen-
577 FITC KC57 (Beckman Coulter) for 1hr at 4°C then washed with PBS and resuspended in FACS
578 buffer (5% FBS in PBS). Events were assessed by flow cytometry on the AttuneNxT (Thermo
579 Fisher Scientific). At least 10,000 events were collected per run. Data was analyzed using FlowJo
580 software.

581

582 **Statistical Analyses**

583 All statistical analyses were performed using GraphPad Prism 9.

584

585 **AUTHOR CONTRIBUTIONS**

586 Conceptualization, C.S. and O.I.F; methodology, C.S.; writing original draft C.S and O.I.F; writing,
587 review and editing C.S. and O.I.F; visualization C.S. and O.I.F.; supervision and funding
588 acquisition O.I.F. All authors have read and agreed to the published version of the manuscript.

589

590 **FUNDING**

591 This work was supported by NIH NIAID grant R01AI147837 to O.I.F. C.S was supported by NIH
592 NIAID F31 Ruth L. Kirschstein National Research Service Award Predoctoral Fellowship F31-

593 AI165286, and the NIH NIGMS Grant GM007185 T32 Ruth L. Kirschstein National Research
594 Service Award Cell and Molecular Biology Training Grant. The funders had no role in study
595 design, data collection and interpretation, or the decision to submit the work for publication.
596
597 **ACKNOWLEDGEMENTS**
598 We like to thank Dr. Julia Mack and Julianne Ashby for their assistance and expertise with Live-
599 cell imaging using the LSM900. We thank Dr. Alexander Hoffmann and Dr. Diane Lefaudeux for
600 her instruction on RNA-seq analysis. We thank Dr. Claudia Lukas for providing U2OS cells that
601 stably express 53PB1-GFP and NBS1-GFP. We thank Dr. Steven Bensinger for the LightCycler
602 480 System, Dr. Jesse Zamudio for the Qubit fluorometer, Dr. Peter Bradley for the Zeiss Axio
603 Imager Z1, Dr. Matteo Pellegrini for the TapeStation, Dr. Steve Jacobsen and Dr. Jefferey Long
604 for the LSM980. We thank Dr. Randilea Nichols Doyle, Karly Nisson, and Vivian Yang for
605 providing comments on the manuscript.
606
607 **COMPETING INTERESTS**
608 The author(s) declare(s) they have no competing interests.

609 **REFERENCES**

610

611 1. Blackford AN, Jackson SP. ATM, ATR, and DNA-PK: The Trinity at the Heart of the DNA
612 Damage Response. Mol Cell. 2017 Jun 15;66(6):801–17.

613 2. Shiloh Y, Ziv Y. The ATM protein kinase: regulating the cellular response to genotoxic stress,
614 and more. Nat Rev Mol Cell Biol. 2013 Apr;14(4):197–210.

615 3. Matthews HK, Bertoli C, de Bruin RAM. Cell cycle control in cancer. Nat Rev Mol Cell Biol.
616 2022 Jan;23(1):74–88.

617 4. Valerie K, Delers A, Bruck C, Thiriart C, Rosenberg H, Debouck C, et al. Activation of human
618 immunodeficiency virus type 1 by DNA damage in human cells. Nature. 1988
619 May;333(6168):78–81.

620 5. Dunphy G, Flannery SM, Almine JF, Connolly DJ, Paulus C, Jønsson KL, et al. Non-
621 canonical Activation of the DNA Sensing Adaptor STING by ATM and IFI16 Mediates NF-κB
622 Signaling after Nuclear DNA Damage. Mol Cell. 2018 Sep 6;71(5):745-760.e5.

623 6. Gorgoulis V, Adams PD, Alimonti A, Bennett DC, Bischof O, Bishop C, et al. Cellular
624 Senescence: Defining a Path Forward. Cell. 2019 Oct 31;179(4):813–27.

625 7. Ryan EL, Hollingworth R, Grand RJ. Activation of the DNA Damage Response by RNA
626 Viruses. Biomolecules. 2016 Jan 6;6(1):2.

627 8. Weitzman MD, Fradet-Turcotte A. Virus DNA Replication and the Host DNA Damage
628 Response. Annu Rev Virol. 2018 Sep 29;5(1):141–64.

629 9. Tachiwana H, Shimura M, Nakai-Murakami C, Tokunaga K, Takizawa Y, Sata T, et al. HIV-1
630 Vpr Induces DNA Double-Strand Breaks. Cancer Res. 2006 Jan 15;66(2):627–31.

631 10. Fregoso OI, Emerman M. Activation of the DNA Damage Response Is a Conserved
632 Function of HIV-1 and HIV-2 Vpr That Is Independent of SLX4 Recruitment. Prasad VR,
633 editor. mBio. 2016 Nov 2;7(5):e01433-16.

634 11. Lang SM, Weeger M, Stahl-Hennig C, Coulibaly C, Hunsmann G, Müller J, et al.
635 Importance of vpr for infection of rhesus monkeys with simian immunodeficiency virus. J
636 Virol. 1993 Feb;67(2):902–12.

637 12. Beaumont T, Van Nuenen A, Broersen S, Blattner WA, Lukashov VV, Schuitemaker H.
638 Reversal of Human Immunodeficiency Virus Type 1 IIIB to a Neutralization-Resistant
639 Phenotype in an Accidentally Infected Laboratory Worker with a Progressive Clinical Course.
640 J Virol. 2001 Mar;75(5):2246–52.

641 13. Balliet JW, Kolson DL, Eiger G, Kim FM, McGann KA, Srinivasan A, et al. Distinct
642 Effects in Primary Macrophages and Lymphocytes of the Human Immunodeficiency Virus
643 Type 1 Accessory Genes vpr, vpu, and nef: Mutational Analysis of a Primary HIV-1 Isolate.
644 Virology. 1994 May 1;200(2):623–31.

645 14. Mashiba M, Collins DR, Terry VH, Collins KL. Vpr Overcomes Macrophage-Specific
646 Restriction of HIV-1 Env Expression and Virion Production. Cell Host Microbe. 2014 Dec
647 10;16(6):722–35.

648 15. Miller CM, Akiyama H, Agosto LM, Emery A, Ettinger CR, Swanstrom RI, et al. Virion-
649 Associated Vpr Alleviates a Postintegration Block to HIV-1 Infection of Dendritic Cells.
650 Sundquist WI, editor. J Virol. 2017 Jul;91(13):e00051-17.

651 16. Paxton W, Connor RI, Landau NR. Incorporation of Vpr into human immunodeficiency
652 virus type 1 virions: requirement for the p6 region of gag and mutational analysis. J Virol.
653 1993 Dec;67(12):7229–37.

654 17. Roshal M, Kim B, Zhu Y, Nghiem P, Planelles V. Activation of the ATR-mediated DNA
655 Damage Response by the HIV-1 Viral Protein R. J Biol Chem. 2003 Jul;278(28):25879–86.

656 18. Zhang F, Bieniasz PD. HIV-1 Vpr induces cell cycle arrest and enhances viral gene
657 expression by depleting CCDC137. eLife. 9:e55806.

658 19. Lahouassa H, Blondot ML, Chauveau L, Chougui G, Morel M, Leduc M, et al. HIV-1 Vpr
659 degrades the HLTF DNA translocase in T cells and macrophages. Proc Natl Acad Sci. 2016
660 May 10;113(19):5311–6.

661 20. Schröfelbauer B, Yu Q, Zeitlin SG, Landau NR. Human Immunodeficiency Virus Type 1
662 Vpr Induces the Degradation of the UNG and SMUG Uracil-DNA Glycosylases. J Virol. 2005
663 Sep;79(17):10978–87.

664 21. Ahn J, Vu T, Novince Z, Guerrero-Santoro J, Rapic-Otrin V, Gronenborn AM. HIV-1 Vpr
665 Loads Uracil DNA Glycosylase-2 onto DCAF1, a Substrate Recognition Subunit of a Cullin
666 4A-RING E3 Ubiquitin Ligase for Proteasome-dependent Degradation *. J Biol Chem. 2010
667 Nov 26;285(48):37333–41.

668 22. Lim ES, Fregoso OI, McCoy CO, Matsen FA, Malik HS, Emerman M. The ability of
669 primate lentiviruses to degrade the monocyte restriction factor SAMHD1 preceded the birth of
670 the viral accessory protein Vpx. Cell Host Microbe. 2012 Feb 16;11(2):194–204.

671 23. Zhou X, DeLucia M, Ahn J. SLX4-SLX1 Protein-independent Down-regulation of
672 MUS81-EME1 Protein by HIV-1 Viral Protein R (Vpr) *♦. J Biol Chem. 2016 Aug
673 12;291(33):16936–47.

674 24. Yan J, Shun MC, Hao C, Zhang Y, Qian J, Hrecka K, et al. HIV-1 Vpr Reprograms CLR4
675 ^{DCAF1} E3 Ubiquitin Ligase to Antagonize Exonuclease 1-Mediated Restriction of HIV-1
676 Infection. Smithgall TE, editor. mBio. 2018 Nov 7;9(5):e01732-18.

677 25. Lv L, Wang Q, Xu Y, Tsao LC, Nakagawa T, Guo H, et al. Vpr Targets TET2 for
678 Degradation by CRL4VprBP E3 Ligase to Sustain IL-6 Expression and Enhance HIV-1
679 Replication. Mol Cell. 2018 Jun 7;70(5):961-970.e5.

680 26. Romani B, Shaykh Baygloo N, Aghasadeghi MR, Allahbakhshi E. HIV-1 Vpr Protein
681 Enhances Proteasomal Degradation of MCM10 DNA Replication Factor through the Cul4-
682 DDB1[VprBP] E3 Ubiquitin Ligase to Induce G2/M Cell Cycle Arrest. J Biol Chem. 2015 Jul
683 10;290(28):17380–9.

684 27. Greenwood EJD, Williamson JC, Sienkiewicz A, Naamati A, Matheson NJ, Lehner PJ.
685 Promiscuous Targeting of Cellular Proteins by Vpr Drives Systems-Level Proteomic
686 Remodeling in HIV-1 Infection. Cell Rep. 2019 Apr 30;27(5):1579-1596.e7.

687 28. Li D, Lopez A, Sandoval C, Nichols Doyle R, Fregoso OI. HIV Vpr Modulates the Host
688 DNA Damage Response at Two Independent Steps to Damage DNA and Repress Double-
689 Strand DNA Break Repair. mBio. 2020 Aug 4;11(4):e00940-20.

690 29. Brzostek-Racine S, Gordon C, Van Scoy S, Reich NC. The DNA Damage Response
691 Induces IFN. J Immunol. 2011 Nov 15;187(10):5336–45.

692 30. Roux P, Alfieri C, Hrimech M, Cohen EA, Tanner JE. Activation of Transcription Factors
693 NF-κB and NF-IL-6 by Human Immunodeficiency Virus Type 1 Protein R (Vpr) Induces
694 Interleukin-8 Expression. J Virol. 2000 May 15;74(10):4658–65.

695 31. Wu ZH, Shi Y, Tibbetts RS, Miyamoto S. Molecular Linkage Between the Kinase ATM
696 and NF-κB Signaling in Response to Genotoxic Stimuli. Science. 2006 Feb
697 24;311(5764):1141–6.

698 32. Huang TT, Wuerzberger-Davis SM, Wu ZH, Miyamoto S. Sequential modification of
699 NEMO/IKKgamma by SUMO-1 and ubiquitin mediates NF-kappaB activation by genotoxic
700 stress. Cell. 2003 Nov 26;115(5):565–76.

701 33. Miyamoto S. Nuclear initiated NF-κB signaling: NEMO and ATM take center stage. Cell
702 Res. 2011 Jan;21(1):116–30.

703 34. Liu R, Lin Y, Jia R, Geng Y, Liang C, Tan J, et al. HIV-1 Vpr stimulates NF-κB and AP-1
704 signaling by activating TAK1. Retrovirology. 2014 Jun 9;11(1):45.

705 35. Kogan M, Deshmane S, Sawaya BE, Gracely EJ, Khalili K, Rappaport J. Inhibition of
706 NF-κB activity by HIV-1 Vpr is dependent on Vpr binding protein. J Cell Physiol. 2013
707 Apr;228(4):781–90.

708 36. Belzile JP, Duisit G, Rougeau N, Mercier J, Finzi A, Cohen ÉA. HIV-1 Vpr-Mediated G2
709 Arrest Involves the DDB1-CUL4AVPRBP E3 Ubiquitin Ligase. PLOS Pathog. 2007 Jul
710 13;3(7):e85.

711 37. Le Rouzic E, Belaïdouni N, Estrabaud E, Morel M, Rain JC, Transy C, et al. HIV1 Vpr
712 arrests the cell cycle by recruiting DCAF1/VprBP, a receptor of the Cul4-DDB1 ubiquitin
713 ligase. Cell Cycle Georget Tex. 2007 Jan 15;6(2):182–8.

714 38. Zhou Y, Zhou B, Pache L, Chang M, Khodabakhshi AH, Tanaseichuk O, et al.
715 Metascape provides a biologist-oriented resource for the analysis of systems-level datasets.
716 Nat Commun. 2019 Apr 3;10(1):1523.

717 39. Russo RC, Garcia CC, Teixeira MM, Amaral FA. The CXCL8/IL-8 chemokine family and
718 its receptors in inflammatory diseases. Expert Rev Clin Immunol. 2014 May 1;10(5):593–619.

719 40. Frazzi R. BIRC3 and BIRC5: multi-faceted inhibitors in cancer. Cell Biosci. 2021 Jan
720 7;11(1):8.

721 41. Mitchell S, Vargas J, Hoffmann A. Signaling via the NFκB system. WIREs Syst Biol Med.
722 2016 May;8(3):227–41.

723 42. Nakai-Murakami C, Shimura M, Kinomoto M, Takizawa Y, Tokunaga K, Taguchi T, et al.
724 HIV-1 Vpr induces ATM-dependent cellular signal with enhanced homologous recombination.
725 Oncogene. 2007 Jan;26(4):477–86.

726 43. Strickland I, Ghosh S. Use of cell permeable NBD peptides for suppression of
727 inflammation. Ann Rheum Dis. 2006 Nov;65(Suppl 3):iii75–82.

728 44. Liang Z, Liu R, Lin Y, Liang C, Tan J, Qiao W. HIV-1 Vpr protein activates the NF-κB
729 pathway to promote G2/M cell cycle arrest. Virol Sin. 2015 Dec 1;30(6):441–8.

730 45. Strebel K. HIV Accessory Proteins versus Host Restriction Factors. Curr Opin Virol.
731 2013 Dec;3(6):10.1016/j.coviro.2013.08.004.

732 46. Lopez A, Nichols Doyle R, Sandoval C, Nisson K, Yang V, Fregoso OI. Viral Modulation
733 of the DNA Damage Response and Innate Immunity: Two Sides of the Same Coin. J Mol
734 Biol. 2022 Mar 30;434(6):167327.

735 47. Virgilio MC, Miguel Disbennett W, Chen T, Lubow J, Welch JD, Collins KL. HIV-1 Vpr
736 combats the PU.1-driven antiviral response in primary human macrophages. BioRxiv Prepr
737 Serv Biol. 2023 Mar 21;2023.03.21.533528.

738 48. Joseph AM, Ladha JS, Mojamdar M, Mitra D. Human immunodeficiency virus-1 Nef
739 protein interacts with Tat and enhances HIV-1 gene expression. FEBS Lett. 2003 Jul
740 31;548(1–3):37–42.

741 49. Sawaya BE, Khalili K, Gordon J, Taube R, Amini S. Cooperative Interaction between
742 HIV-1 Regulatory Proteins Tat and Vpr Modulates Transcription of the Viral Genome *. J Biol
743 Chem. 2000 Nov 10;275(45):35209–14.

744 50. Bauby H, Ward CC, Hugh-White R, Swanson CM, Schulz R, Goujon C, et al. HIV-1 Vpr
745 Induces Widespread Transcriptomic Changes in $CD4^+$ T Cells Early Postinfection. Goff SP,
746 editor. mBio. 2021 Jun 29;12(3):e01369-21.

747 51. Chougui G, Munir-Matloob S, Matkovic R, Martin MM, Morel M, Lahouassa H, et al. HIV-
748 2/SIV viral protein X counteracts HUSH repressor complex. Nat Microbiol. 2018
749 Aug;3(8):891–7.

750 52. Yurkovetskiy L, Guney MH, Kim K, Goh SL, McCauley S, Dauphin A, et al. Primate
751 immunodeficiency virus proteins Vpx and Vpr counteract transcriptional repression of
752 proviruses by the HUSH complex. Nat Microbiol. 2018 Dec;3(12):1354–61.

753 53. Cicchini L, Westrich JA, Xu T, Vermeer DW, Berger JN, Clambey ET, et al. Suppression
754 of Antitumor Immune Responses by Human Papillomavirus through Epigenetic
755 Downregulation of CXCL14. Imperiale MJ, editor. mBio. 2016 Jul 6;7(3):e00270-16.

756 54. Romero N, Favoreel HW. Pseudorabies virus infection triggers NF-κB activation via the
757 DNA damage response, but actively inhibits NFkB-dependent gene expression. J Virol. 2021
758 Oct 6;JVI.01666-21.

759 55. Harman AN, Nasr N, Feetham A, Galoyan A, Alshehri AA, Rambukwelle D, et al. HIV
760 Blocks Interferon Induction in Human Dendritic Cells and Macrophages by Dysregulation of
761 TBK1. Silvestri G, editor. J Virol. 2015 Jul;89(13):6575–84.

762 56. Gummuluru S, Emerman M. Cell Cycle- and Vpr-Mediated Regulation of Human
763 Immunodeficiency Virus Type 1 Expression in Primary and Transformed T-Cell Lines. J Virol.
764 1999 Jul;73(7):5422–30.

765 57. Goh WC, Rogel ME, Kinsey CM, Michael SF, Fultz PN, Nowak MA, et al. HIV-1 Vpr
766 increases viral expression by manipulation of the cell cycle: A mechanism for selection of Vpr
767 in vivo. Nat Med. 1998 Jan;4(1):65–71.

768 58. Nodder SB, Gummuluru S. Illuminating the Role of Vpr in HIV Infection of Myeloid Cells.
769 Front Immunol [Internet]. 2019 [cited 2023 Apr 3];10. Available from:
770 https://www.frontiersin.org/articles/10.3389/fimmu.2019.01606

771 59. Varin A, Decrion AZ, Sabbah E, Quivy V, Sire J, Van Lint C, et al. Synthetic Vpr Protein
772 Activates Activator Protein-1, c-Jun N-terminal Kinase, and NF-κB and Stimulates HIV-1
773 Transcription in Promonocytic Cells and Primary Macrophages*. J Biol Chem. 2005 Dec
774 30;280(52):42557–67.

775 60. Fabryova H, Kao S, Sukegawa S, Miyagi E, Taylor L, Ferhadian D, et al. HIV-1 Vpr
776 Induces Degradation of Gelsolin, a Myeloid Cell-Specific Host Factor That Reduces Viral
777 Infectivity by Inhibiting the Expression and Packaging of the HIV-1 Env Glycoprotein. Goff
778 SP, editor. mBio. 2023 Feb 28;14(1):e02973-22.

779 61. Bruce JW, Bracken M, Evans E, Sherer N, Ahlquist P. ZBTB2 represses HIV-1
780 transcription and is regulated by HIV-1 Vpr and cellular DNA damage responses. PLOS
781 Pathog. 2021 Feb 26;17(2):e1009364.

782 62. Yamashita M, Emerman M. Capsid Is a Dominant Determinant of Retrovirus Infectivity in
783 Nondividing Cells. J Virol. 2004 Jun;78(11):5670–8.

784 63. Choi VW, Asokan A, Haberman RA, Samulski RJ. Production of Recombinant Adeno-
785 Associated Viral Vectors for In Vitro and In Vivo Use. Curr Protoc Mol Biol [Internet]. 2007
786 Apr [cited 2023 May 3];78(1). Available from:
787 https://onlinelibrary.wiley.com/doi/10.1002/0471142727.mb1625s78

788 64. Bekker-Jensen S, Lukas C, Melander F, Bartek J, Lukas J. Dynamic assembly and
789 sustained retention of 53BP1 at the sites of DNA damage are controlled by Mdc1/NFBD1. J
790 Cell Biol. 2005 Jul 18;170(2):201–11.

791 65. Lukas C, Melander F, Stucki M, Falck J, Bekker-Jensen S, Goldberg M, et al. Mdc1
792 couples DNA double-strand break recognition by Nbs1 with its H2AX-dependent chromatin
793 retention. EMBO J. 2004 Jul 7;23(13):2674–83.

794

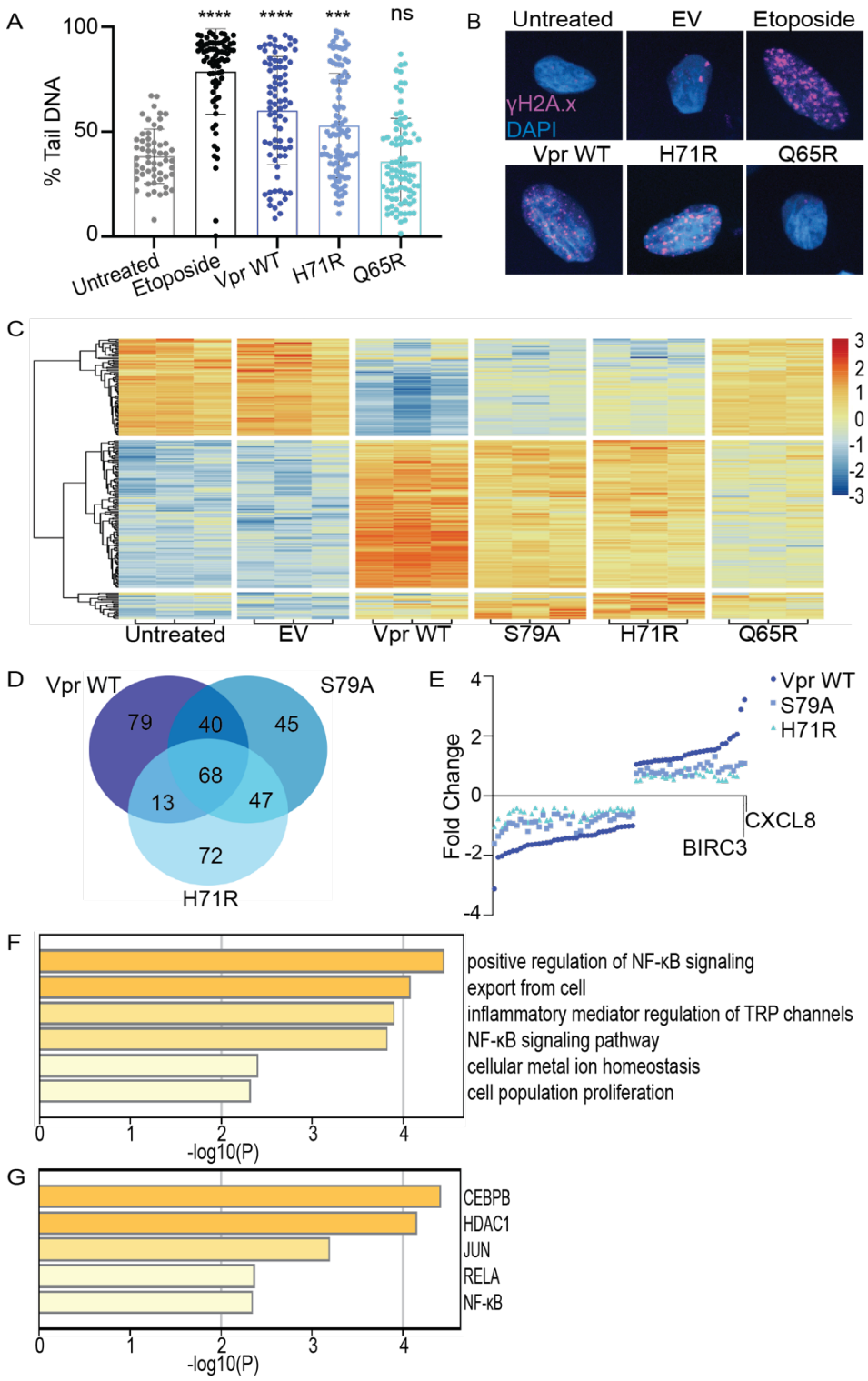

Figure 1: HIV-1 Vpr induces DNA damage and alters cellular transcription independent of cell cycle arrest and CRL4A^{DCAF1} engagement. (A) Comet assay of U2OS cells infected with rAAV expressing 3xFLAG-tagged Vpr WT, H71R, Q65R, untreated (negative control), or 50uM etoposide (positive control). Percent tail DNA was quantified at 24 hours post infection (hpi) using the OpenComet plug-in for the ImageJ software. Each circle represents one cell. N=3, one

802 representative experiment shown. (B) Representative immunofluorescence images of U2OS cells
803 infected under the same conditions as Fig. 1A; γH2A.x (magenta) and nuclei stained with DAPI
804 (blue). Images were taken at 63x magnification. N=3, one representative experiment shown. EV,
805 empty vector. (C) RNA-seq of U2OS cells at 36 hpi. Heat map displays Log_2 fold changes of
806 upregulated genes in red and downregulated genes in blue. Each column represents a biological
807 replicate, n=3 (D) Venn diagram of the top 100 upregulated and top 100 downregulated genes
808 among Vpr WT, S79A, H71R, and Q65R. E) Dot plot of the 68 conserved differentially expressed
809 genes among Vpr WT, S79A, and H71R. BIRC3 and CXCL8 are highlighted as the two most
810 upregulated genes (Log_2 fold change) under all conditions. (F) Gene ontology and (G) TRRUST
811 analysis of the 30 upregulated genes performed with Metascape software. Asterisk indicate
812 statistical significance compared to untreated control, as determined by one-way ANOVA test
813 (NS, nonsignificant; *** $P< 0.0004$, **** $P< 0.0001$). Related to Figures S1 and S2.

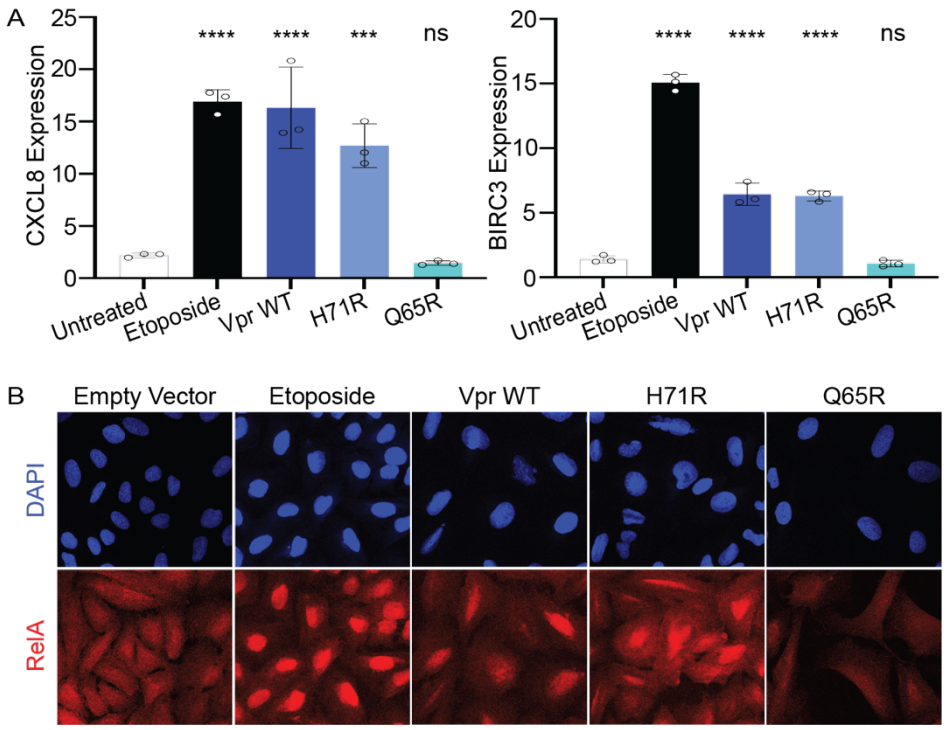

Figure 2: HIV-1 Vpr activates RelA and promotes NF-κB transcription independent of cell cycle arrest and CRL4A^{DCAF1} engagement. (A) qRT-PCR validation of upregulated NF-κB target genes BIRC3 and CXCL8. Normalized expression (ΔΔCt) was calculated by normalizing to GAPDH followed by calculating fold change to untreated or empty vector treated cells. Cells treated under the same conditions as Fig. 1C. n=3, one representative experiment shown. (B) Representative immunofluorescence images of U2OS cells infected under the same conditions as Fig. 1A; RelA (red) and nuclei stained with DAPI (blue). Images were taken at 63x magnification. n=3, one representative experiment shown. Asterisk indicate statistical significance compared to untreated control, as determined by one-way ANOVA test (NS, nonsignificant; *** P< 0.0003, **** P< 0.0001).

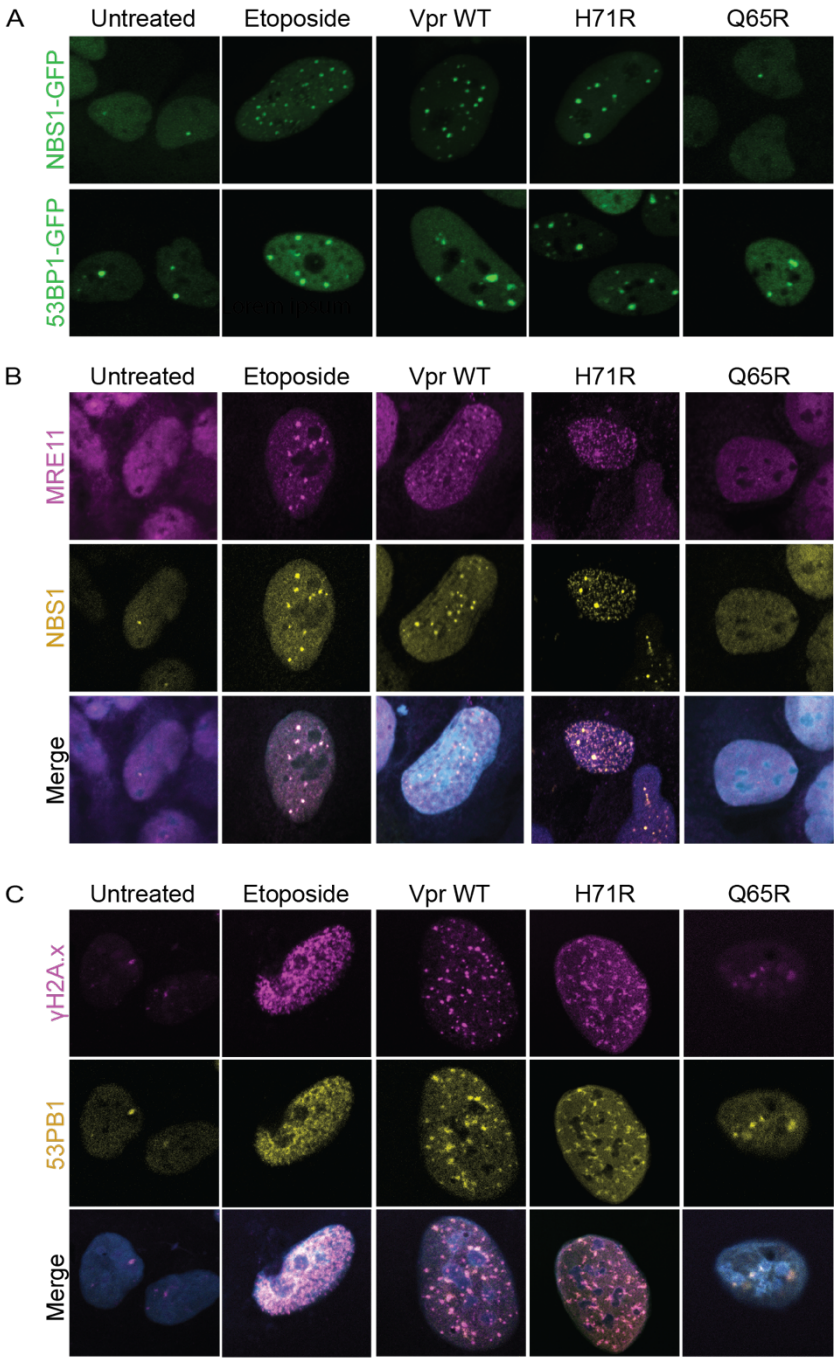

Figure 3: Vpr-induced DNA damage activates ATM signaling independent of cell cycle arrest and CRL4A^{DCAF1} engagement. (A) Live-cell imaging of U2OS cells stably expressing NBS1-GFP or 53PB1-GFP. Cells were infected under the same conditions as Fig. 1A and representative images were taken at 33 hpi at 63x magnification. n=3, one representative experiment shown. (B) Representative images of co-localization of DNA damage sensors MRE11 (magenta) and NBS1 (yellow) in U2OS NBS1-GFP or (C) DNA damage transducers γH2A.x (magenta) and 53PB1 (yellow) in U2OS 53PB1-GFP cells infected under the same conditions as Fig. 1A. Representative images taken at 24 hpi at 63x magnification. n=3, one representative experiment shown. Related to Figure S3.

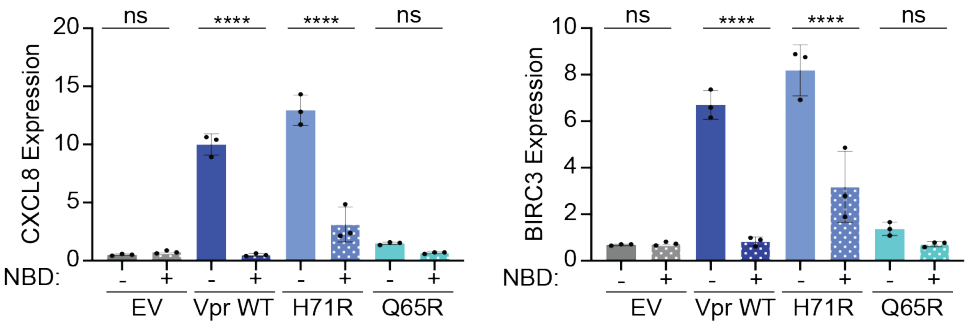

Figure 4: Vpr upregulates NF-κB transcription dependent on NEMO, yet independent of cell cycle arrest and CRL4A^{DCAF1} engagement. qRT-PCR of BIRC3 and CXCL8 in the presence or absence of Nemo-Binding Inhibitor peptide (NBD) at 36 hpi. U2OS cells were pretreated with 100uM of NBD for 2 hours prior to infection with rAAV expressing 3xFLAG-tagged Vpr WT, H71R, Q65R, empty vector (negative control). Normalized expression to GAPDH. Asterisk indicate statistical significance compared to untreated control, as determined by one-way ANOVA test (NS, nonsignificant; **** P< 0.0001).

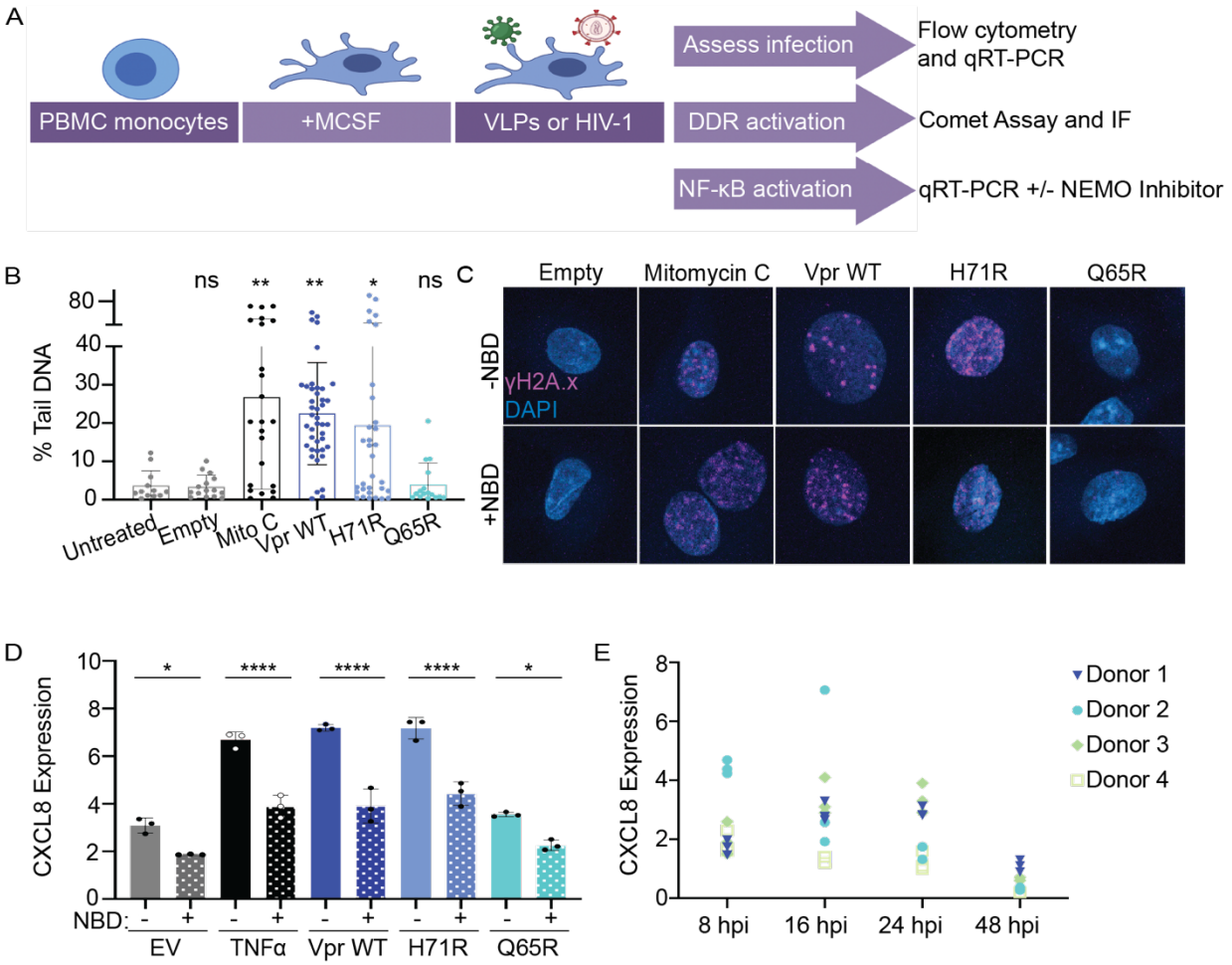

Figure 5: Vpr-induced DNA damage activates ATM-NEMO signaling and NF-κB transcription in primary MDMs early during infection. (A) Experimental schematic depicting the isolation and differentiation of primary human monocyte-derived macrophages (MDMs) from peripheral blood mononuclear cells (PBMCs) followed by delivery of Vpr via Virus-like Particles (VLPs) or HIV-1 infection. Infected MDMs were assayed for induction of DNA damage, activation of DDR signaling, and the upregulation of NF-κB target genes in the context of NEMO inhibitor. (B) Comet assay of MDMs treated with VLPs packaging 3xFLAG-tagged Vpr WT, H71R, Q65R, empty VLPs (negative control), or 25uM Mitomycin C (positive control) for 8 hours. Comet assay analysis was performed as in Fig. 1A. n=2, one representative experiment shown. (C) Representative immunofluorescence images of MDMs infected with VLPs as in Fig. 5B and treated or not with Nemo-Binding Inhibitor peptide (NBD); γH2A.x (magenta) and nuclei stained with DAPI (blue). Images were taken at 100x magnification. n=3, one representative experiment shown. (D) qRT-PCR for CXCL8 of MDMs treated with NBD as in Fig. 5C with TNFα as positive control. n=3, one representative experiment shown. (E) qRT-PCR for CXCL8 of MDMs infected with HIV-1 ΔEnv for 8, 16, 24, and 48 hpi from four separate donors. Normalized expression to GAPDH. Asterisk indicate statistical significance compared to untreated control, as determined by one-way ANOVA test (NS, nonsignificant; * P<0.03, ** P < 0.005, **** P< 0.0001). Related to Figure S4.

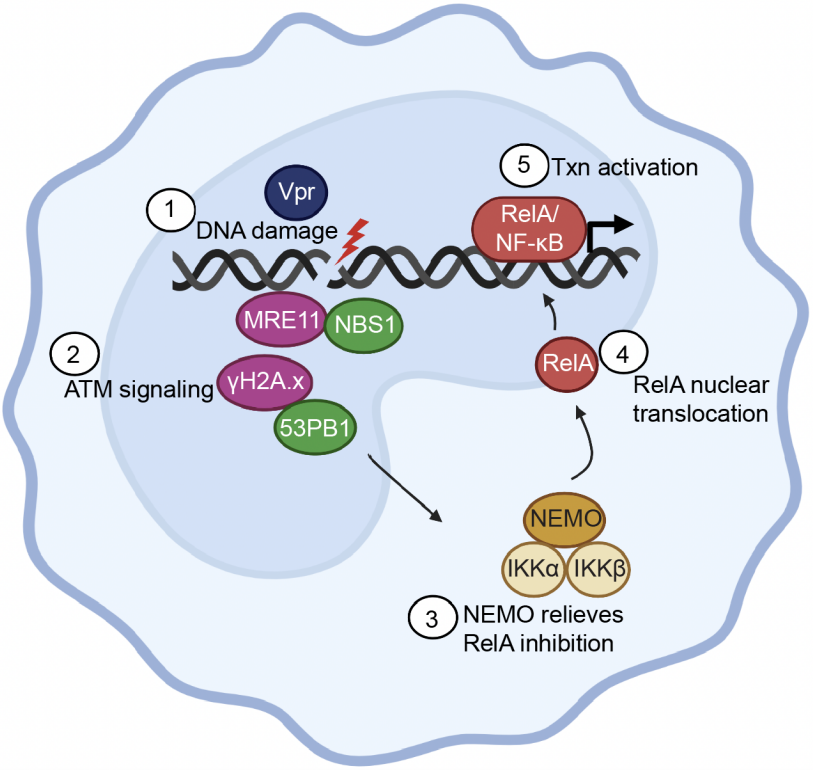

Figure 6: Model showing Vpr-induced DNA damage activates ATM and NEMO signaling resulting in RelA nuclear translocation and NF-κB transcriptional upregulation. 1. Vpr induces double-strand DNA breaks independent of cell cycle arrest and CRL4A^{DCAF1} complex engagement. 2. Vpr-induced DNA damage activates markers of ATM signaling including MRE11, NBS1, γH2A.x, and 53PB1. 3. ATM-DDR activation results in NEMO relieving RelA inhibition from inhibitor of NF-κB (IκBα and IκBβ). 4. RelA translocates into the nucleus. 5. RelA binds to NF-κB promoters and activates transcription (txn) of NF-κB target genes such as BIRC3 and CXCL8. (Schematic made on Biorender).

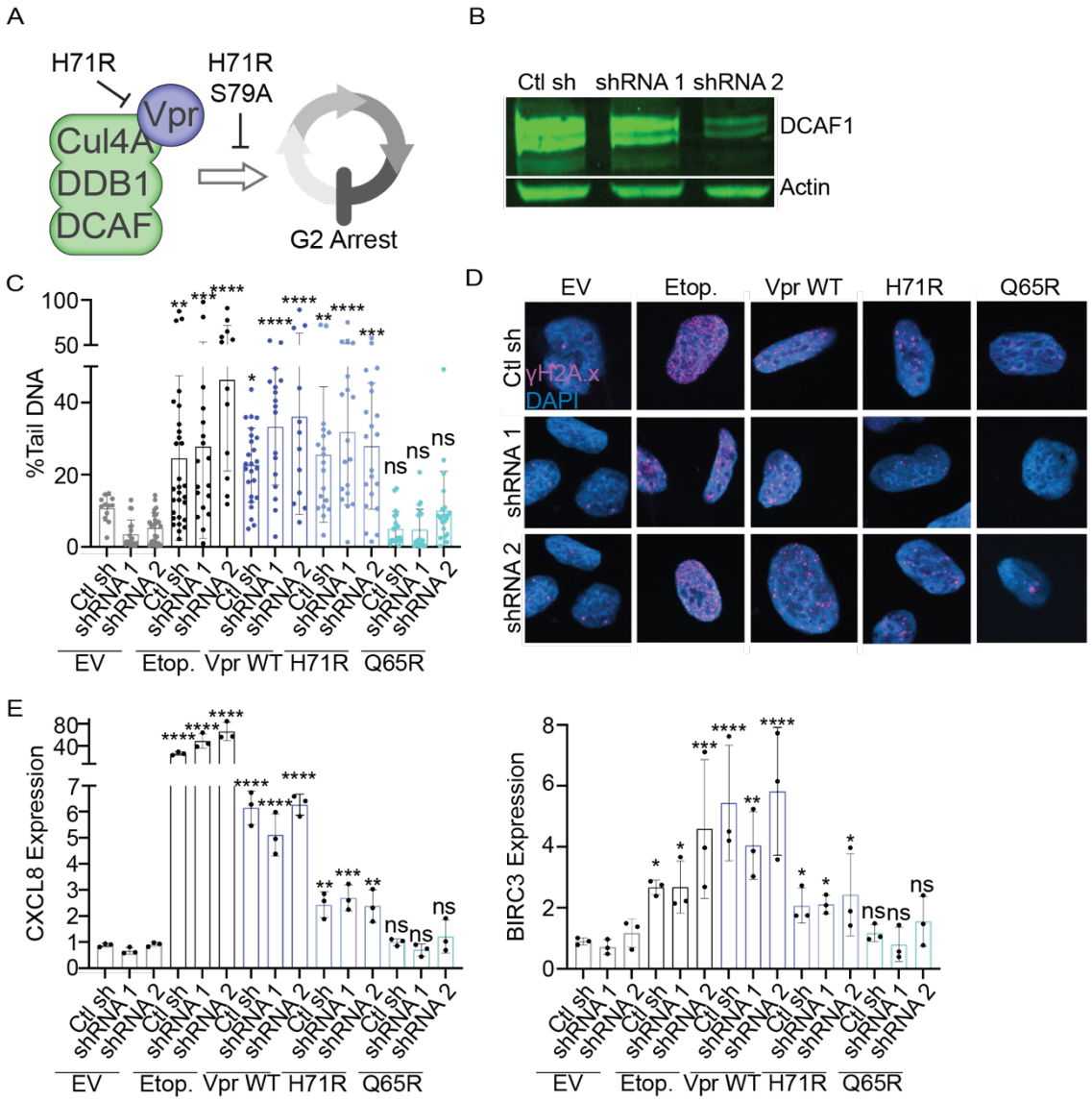

Figure S1: Knockdown of DCAF1 does not abrogate the ability of Vpr to induce DNA damage, activate DDR signaling, or upregulate NF-κB target genes. (A) Schematic representation of Vpr mutants used in these studies to decouple some Vpr functions. Vpr S79A and Vpr H71R do not induce cell cycle arrest, and H71R also does not bind DCAF1 of the CRL4A^{DCAF1} complex to degrade host proteins or remodel the proteome. Vpr Q65R (not shown) is a largely non-functional negative control. (B) Western blot of endogenous DCAF1 U2OS cells to test stable knockdown with shRNA. Control (ctl) shRNA and two DCAF1-specific shRNAs (shRNA1 and shRNA2) were used. Actin is used as a loading control. (C) Comet assay of DCAF1 knock-down cells infected with rAAV and analyzed as in Fig. 1A. n=1. (D) Representative immunofluorescence images of DCAF1 knock-down U2OS cells infected under the same conditions as Fig. 1A.; γH2A.x (magenta) and nuclei with DAPI (blue). Images were taken at 63x magnification. n=1, one representative image shown. (E) qRT-PCR for CXCL8 and BIRC3 in DCAF1 knock-down U2OS cells infected under the same conditions as Fig. 1A. n=1. Asterisk indicate statistical significance compared to untreated control, as determined by t-test (NS, nonsignificant; * P< 0.02, ** P<0.004, *** P<0.0003, **** P<0.0001). EV, empty vector negative control; Etop., etoposide positive control. Related to Figures 1 and 2.

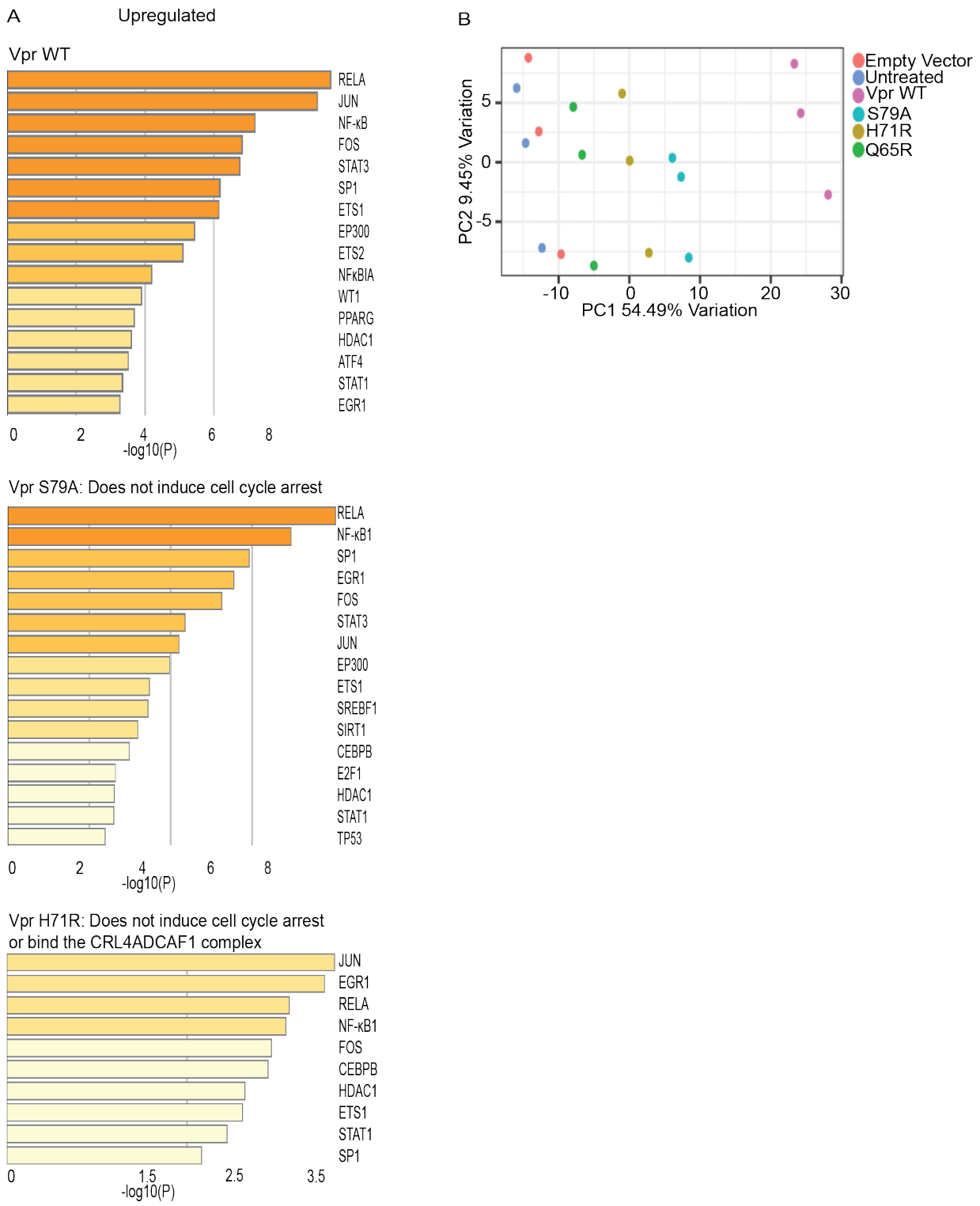

Figure S2: Vpr alters cellular transcription through diverse mechanisms that are either dependent or independent of cell cycle arrest and CRL4A^{DCAF1} engagement. (A) Gene ontology using Metascape displaying TRRUST analysis for upregulated genes. (B) Principal component analysis (PCA) of the RNA-seq data showing the relatedness of the three biological replicates compared to empty vector or untreated cells. Related to Figure 1.

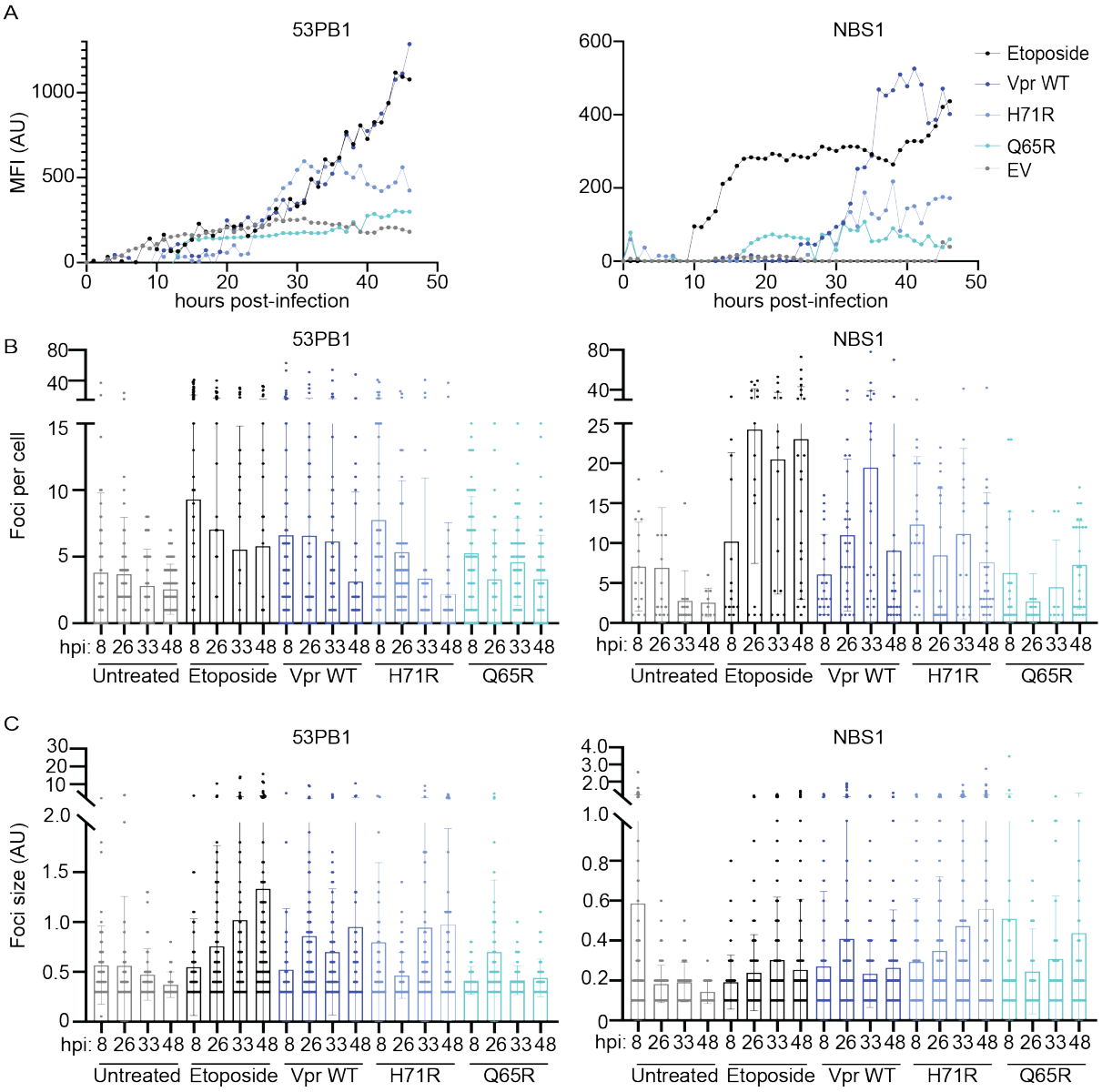

Figure S3: Vpr-induced DNA damage activates markers of ATM signaling. (A) Live-cell imaging taken on the IncuCyte of U2OS NBS1-GFP or 53PB1-GFP cells infected as in Fig. 1A for 48 hrs. n=2, one representative experiment shown. (B & C) Quantification of DNA damage induced in the live-cell imaging experiment in Fig. 3A at 8, 26, 33, and 48hpi. Foci per cell and foci size were quantified using ImageJ software. Images were taken at 63x magnification using the LSM 900. n=3, one representative experiment shown. EV, empty vector; AU, arbitrary units. Related to Figure 3.

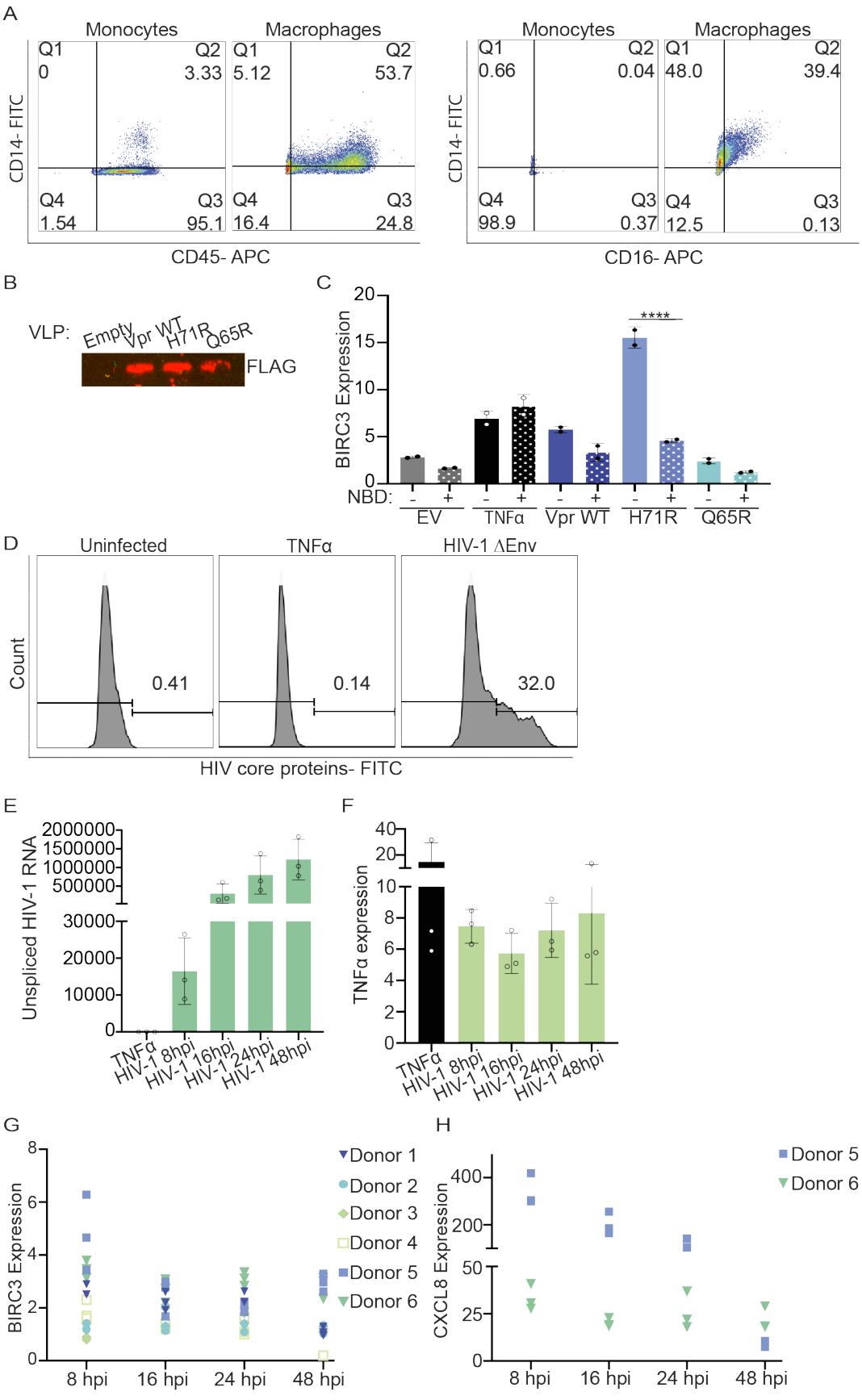
A
Monocytes
Macrophages
Q1 0
Q2 3.33
Q4 1.54
Q3 95.1
Q1 5.12
Q2 53.7
Q4 16.4
Q3 24.8
CD14- FITC
CD45- APC
Monocytes
Macrophages
Q1 0.66
Q2 0.04
Q4 98.9
Q3 0.37
Q1 48.0
Q2 39.4
Q4 12.5
Q3 0.13
CD16- APC
B
VLP: Empty Vpr WT H71R Q65R
FLAG
C
BIRC3 Expression
****
NBD: - + - + - + - + - +
EV TNFα Vpr WT H71R Q65R
D
Uninfected
TNFα
HIV-1 ΔEnv
Count
0.41
0.14
32.0
HIV core proteins- FITC
E
Unspliced HIV-1 RNA
TNFα
HIV-1 8hpi
HIV-1 16hpi
HIV-1 24hpi
HIV-1 48hpi
F
TNFα expression
TNFα
HIV-1 8hpi
HIV-1 16hpi
HIV-1 24hpi
HIV-1 48hpi
G
BIRC3 Expression
Donor 1
Donor 2
Donor 3
Donor 4
Donor 5
Donor 6
8 hpi
16 hpi
24 hpi
48 hpi
H
CXCL8 Expression
Donor 5
Donor 6
8 hpi
16 hpi
24 hpi
48 hpi

908

909 **Figure S4: Infection of primary MDMs with VLPs packaging Vpr protein or HIV-1 infection**
910 **upregulate NF-κB transcription dependent on NEMO.** (A) Flow cytometry plots displaying
911 differentiation of PBMC-derived monocytes to macrophages. Primary MDMs are CD14+, CD45+
912 and CD16+. n=6, one representative experiment shown. (B) Western blot of 3X FLAG-Vpr WT
913 and mutants packaged in Virus-like particles (VLPs). (C) qRT-PCR for BIRC3 of MDMs treated
914 with NBD as in Fig. 5C with TNFα as positive control. n=3, one representative experiment
915 shown. (D) Histogram quantifying percent of infected MDMs with HIV-1 ΔEnv at 48hpi. n=6, one
916 representative experiment shown. (E) qRT-PCR for unspliced HIV-1 RNA at 8, 16, 24 and
917 48hpi. n=6, one representative experiment shown. (F) qRT-PCR for TNFα of MDMs infected
918 with HIV-1 ΔEnv at 8, 16, 24 and 48hpi. n=6, one representative experiment shown. (G & H)
919 qRT-PCR for BIRC3 or CXCL8 of MDMs infected with HIV-1 ΔEnv at 8, 16, 24 and 48hpi in
920 separate donors. n=6, (G) is all 6 donors, (H) is donors 5 and 6 in addition to those shown in
921 Fig. 5E. Asterisk indicate statistical significance compared to untreated control, as determined
922 by one-way ANOVA test (NS, nonsignificant; **** P<0.0001). Related to Figure 5.